SILICON CONCENTRATION SOLAR CELL
ANALYSIS OF RESISTANCE FOR HIGH LIGHT INTENSITY USE

by

Kenneth Donald McAlpine

A Thesis Submitted to the Faculty of the

DEPARTMENT OF ELECTRICAL ENGINEERING

In Partial Fulfillment of the Requirements
For the Degree of

MASTER OF SCIENCE

In the Graduate College

THE UNIVERSITY OF ARIZONA

1977

STATEMENT BY AUTHOR

This thesis has been submitted in partial fulfillment of requirements for an advanced degree at The University of Arizona and is deposited in the University Library to be made available to borrowers under rules of the Library.

Brief quotations from this thesis are allowable without special permission, provided that accurate acknowledgment of source is made. Requests for permission for extended quotation from or reproduction of this manuscript in whole or in part may be granted by the head of the major department or the Dean of the Graduate College when in his judgment the proposed use of the material is in the interests of scholarship. In all other instances, however, permission must be obtained from the author.

SIGNED: Kenneth D McElgine

APPROVAL BY THESIS DIRECTOR

This thesis has been approved on the date shown below:

Reginald Lessey Call
Reginald Lessey Call
Associate Processor of
Electrical Engineering

14 July 1977
Date

ACKNOWLEDGMENTS

I wish to thank the Electrical Engineering Solid State Laboratory personnel for their help and the use of the equipment in the laboratory.

Part of the data was gained while under a NASA Contract Number NCA2-OR040-502. I wish to acknowledge their monetary support.

TABLE OF CONTENTS

LIST OF ILLUSTRATIONS

LIST OF ILLUSTRATIONS--Continued.

LIST OF TABLES

LIST OF TABLES--Continued.

ABSTRACT

The use of concentration to increase the power output of a solar cell has evolved as the semiconductor industry has increased the purity of the processing equipment. After raising the material limits, the new low resistivity material was found to maintain high efficiency under concentration due to the decrease in bulk resistivity. A model for high intensity design was made and then the patterns were fabricated. The range of testing was over an intensity of 100 mw/cm^2 to 20 watts/cm^2 and a temperature range of 20^{o}C to 150^{o}C. The experimentally determined resistance of the thirty finger per centimeter pattern with two mains was fourteen thousandths of an ohm. The fourty-five finger per two centimeters had a high efficiency under a light flux of 1.1 watts/cm^2 of twelve percent at 44^{o}C. The maximum power output was 130 times the one sun power at an intensity of 160 times the one sun value with a temperature of 115^{o}C.

CHAPTER 1

INTRODUCTION

The use of the sun for electrical power has been a dream for many years. The decreasing fossil fuel reserves indicate that other sources of energy will be needed. The sun shines enough energy on the surface of the earth to run every process currently in production.

I believe that the cost reductions achieved by using concentration solar cells is one way for medium-scale power production to compete with current power production for medium-scale power plants.

The discovery of the basic effects behind the operation of solar cells has spanned approximately 100 years. It started with the discovery of selenium in 1817 by Berzelius, who was the first to prepare elemental silicon a few years later. This was followed in 1839 by Edmond Becquerel's discovery of the photovoltaic effect. Becquerel noticed that a voltage was produced when one electrode was illuminated in an electrolytic cell. Then in 1873, Willoughby Smith made the discovery of photoconductivity in selenium. This latter event spawned a flurry of activity which included the discovery of the spectral sensitivity of selenium photoconductors, the proposal of a light meter, and the observation of the photovoltaic effect in a solid-state selenium structure by W. G. Adams and R. E. Day in 1876.

Seven years later, the first selenium photovoltaic cell was described by Fritts, who in 1885 attempted the simulation of the human

eye response by a combination of selenium cells and color filters. Then in 1904, the photosensitivity of copper cuprous-oxide structures was observed by Hallwacks, and in 1914, the photovoltaic effect was for the first time connected with the existence of a barrier layer.

In 1917, the first single crystal growth from a melt, the Czochralski Method, was perfected. The perfection of the selenium device came on the heels of the copper-cuprous-oxide device. The front wall selenium device has conversion efficiencies of one percent which was an order of magnitude over the copper-cuprous-oxide device.

From 1920 to 1950, many explanations were found for the semiconductor behavior. "The Theory of Solids" by Strut and Brillouin, Kronig and Penny; "Valence and Hole Barrier Cell" by Schottky; "Electron Diffusion Theory" by Dember; "Cell Characterization (Se, $Cu-Cu_2O$, PbS) for Photometry Application" by Lange; "Metal-Semiconductor Barrier Theory" by Mott and Schottky; and "P-N Junction Theory" by Shockley were theories that opened the beginning of the semiconductor field.

In 1941, the change from selenium occurred with a one percent efficiency Thallium-Sulfide device.

With the progressing development of the silicon technology, the "grown P-N junction technique" led to the preparation of a silicon single crystal photovoltaic device in 1941. It was not until twelve years later when the technology for impurity diffusion of P-N junctions that the silicon solar cell became a practical device.

In 1954, researchers turned to the problem of utilizing the photovoltaic effect as a source of power. In that year, Pearson,

Fuller, and Chapin at Bell Telephone Laboratories made a cell with a conversion efficiency of six percent. Within another two years, RCA and other private industrial companies started production of P-N junctions with the two types of semiconductors. Fabrication process improvements, improved the understanding of the theory of device operation and improved the design of the device, leading to gradually increasing efficiencies which reached fourteen percent efficiency in terrestrial sunlight by 1958.

From that point on, the prime engineering effort has shifted toward adapting the cells to space power systems, improving their reliability and in particular their resistance to nuclear particle radiation, and reducing the fabrication cost.

Solar radiation was first used as a source of electricity in space by the U. S. Satellite Vanguard I, which was put into orbit on March 17, 1958, carrying 108 silicon solar cells in six groups of 18 cells each. Radiation encountered in the Van Allen belts caused the cells to deteriorate, but in the mid-1960's they continued to transmit intelligible signals. Subsequent satellites and space vehicles have used much larger numbers of cells arranged in series-parallel circuits so that they could charge sealed storage batteries and, thus, provide relatively large amounts of power for short periods of transmission. The current uses for terrestrial cells have proven that in remote locations it is practical to use solar cells, and the reliability has been high.

CHAPTER 2

PHOTOVOLTAIC EFFECT

When photons are incident with energy greater than the band-gap, absorption of the photons can take place and electrons can be raised in energy from the valence band to the conduction band, creating hole-electron pairs. If the excess minority carriers (holes on the N-side and electrons on the P-side of the junction) are able to diffuse to the edges of the space charge region before they recombine, they are "swept" across the junction, giving rise to a photocurrent, photovoltage, and power into the load.

The preferential separation of holes and electrons under no exterior load causes a charge build-up in the built-in field until a steady state recombination rate occurs across the junction equal to the hole-electron pairs created per square centimeter per second. This resulting maximum voltage is called the open circuit voltage, denoted by the symbol V_{oc}. If the charges are drained off with a short metallic wire, the resulting current in this wire is called the short-circuit current, I_{sc}, and the magnitude is equivalent in the ideal photovoltaic generator model to the light current, I_L.

The only carriers that influence the V_{oc}, I_{sc} are the carriers that diffuse into the depletion region from the N-type and P-type sides before recombining. The charge carriers are the minority carrier in the doped silicon semiconductor. The length in the respective type

material that the minority carrier can diffuse is called the diffusion length. The diffusion length depends on the material and the impurity concentrations present in the semiconductor. The impurity doping of the N-type or P-type atoms is inversely proportional to the diffusion length of the minority carriers.

In building the model, let us first consider the diode equation.

$$I_j = qA(P_N L_P/T_P + N_P L_N/T_N)(\exp(qV/KT) - 1) \text{ (Fig. 1)} \qquad (1)$$

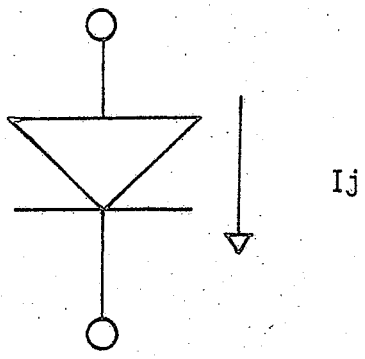

Fig. 1. Diode.

The symbols are the following: q is the electronic charge; A is the area of the junction; L_P is the diffusion length of the holes in the N-side; L_N is the diffusion length of the electrons in the P-side; T_P is the lifetime of holes in a N-type semiconductor; T_N is the lifetime of electrons in a P-type semiconductor; P_N is the holes in the N-side and is dependent on the doping; N_P is the electrons in the P-side and is also dependent on the doping level; V is the voltage across the junction; K is the Boltzman constant; and I_j is the resulting diode current.

The equivalent circuit which represents an Ideal Photovoltaic Generator is shown in Fig. 2,[1]

Where I is the current entering the terminal, V is the voltage measured at the terminals, I_j is the junction current, and I_L is the light generated current.

This is all that is needed for the consideration in the nest chapter of the non-ideal characteristics due to internal resistance.

$$I = I_j - I_L \tag{2}$$

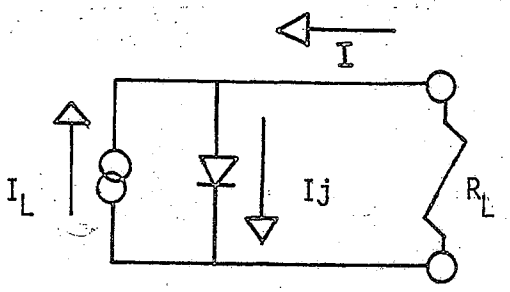

Fig. 2. Ideal Solar Cell Model.

---

1. Paul Rappaport, "The Photovoltaic Effect," RCA Review, Vol. 20, September, 1959, pp. 373-397.

CHAPTER 3

THE NON-IDEAL EFFECTS

Flux Equation Approximation

The solar cell is a photovoltaic generator that is used to collect its photons from the spectrum of the sun. The characteristics are influenced by the antireflection coating, the semiconductor surface states, the wavelength properties, the diffusion length--which is shortened by impurities, and the collection efficiency of the generated minority carriers. These factors are inherent to the actual semiconductor that instead of considering each of these parameters as design considerations, I introduce instead an experimental expression:

$$F = I_L/A \tag{3}$$

with the provision that I_L is measured with the same area for the front contact as in the final design covered with the metal pattern and that the light flux be of the solar spectrum with a power of one hundred milliwatts per square centimeter. The term F is in amps per square centimeter and is approximately 0.025 amps/square centimeter.

The actual spectral qualities are very important to the efficiency. The antireflection coatings would also be a study; and, so, to simplify, a method of cancellation was devised. For each junction depth and profile, the spectral characteristics change. When the junction is made thinner to the surface of the incoming light with the

junction perpendicular to the light flux, the photocurrent sees a rise in the collection efficiency in the blue end of the spectrum. The resulting problem is then the surface states and losses due to a higher lateral resistivity. This shows that in the design of a solar cell tradeoffs must be made in the effort of lowering the losses.

The choosing of a junction profile and depth with an antireflection coating and thickness allows the variables to be measured in a lumped value for the light generated current density so that the spectral characteristics can be cancelled out of the measured cells except as the shadowing of the particular pattern of metal mains and fingers on the solar cells front contact. This allows an analysis simplification and a greater emphasis on the design variables.

The design should maximize the light current and give the highest efficiency with the consistency of the process held high. The fabrication of the cells took months, so the variables of the process had to be closely controlled. The result was a choice of 1Ω-cm boron doped wafers with a junction profile put in at 920°C giving a sheet resistivity of 20Ω/□, and a measured junction depth of 0.4 μm. The result of the processing was sixty wafers of varying light current densities of 25 ma/cm^2 ± 1.3 ma/cm^2 at 100 mw/cm^2 of solar spectrum input flux.

The Environmental Effects

During testing, the days were chosen to be clear with very low humidity. The wafers to be tested were first calibrated with a standard JPL cell to 100 mw/cm^2 on a cooled base. After calibration, this

light current was called the one sun value for the test wafer. The number of suns was then calculated by dividing the one sun current into the light current generated. Since the light current does change with the spectrum, and the spectrum is affected by the water vapor in the atmosphere, the inaccuracies caused by the increase in intensity due to the water vapor is compensated by the water-cooled base to remove the extra heat generated in the cell. Since the temperature would try to rise a few degrees Kelvin, the current change per degree is important to know. The result for a five degree rise is a 0.4 percent change in the short circuit current. This temperature dependence will be handled later.

The moisture in the air has another effect. That is the effect of corrosion on the contact. Since we use different metals on the wafer contacts, galvanic corrosion could occur.

In humidity and long periods of time, the titanium-silver contact does have a corrosion problem. This contact degradation has caused the whole contact system to be studied by R. Gereth and H. Fischer.[2]

The degradation of the solar cell performance is caused by local electrochemical elements at the Ti-Ag interface. Titanium at the interface is dissolved anodically. This corrosion reaction leads to the formation of an interface layer between the titanium and silver, consisting of titanium oxides. The rate at which this affects the

---

2. R. Gereth, H. Fisher, E. Link, S. Mattes, and W. Pschunder, "Contribution to Silicon Solar Cell Technology," Energy Conversion, Vol. 12, September 1972, pp. 103-107.

resistance in 100 percent relative humidity and with a temperature of 90°C is 100 hours to doubling of the resistance and 300 hours to complete failure.

The way to prevent this failure is to put a layer of palladium between the titanium and silver. The result is that after two years no degradation occurred in the cell after being tested in the hot and humid environment.[3]

The Ideal and Real I-V Characteristics

The ideal characteristics of the solar cell is a current source in parallel with a diode. The characteristics will be a shifted diode curve as shown in Fig. 3.

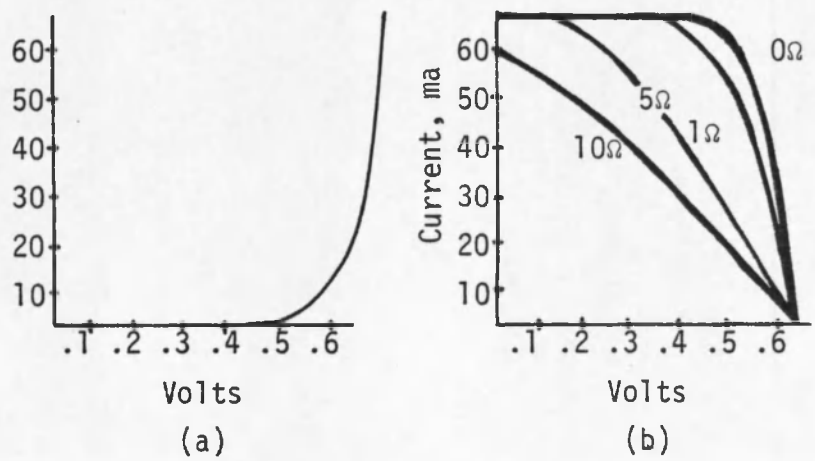

Fig. 3. (a) Ideal Diode; (b) The Effect of Series Resistance with the Curve for the Fourth Quadrant Shifted to the First by Multiplying the Current by -1.

---

3. Gereth et al.

The real cell has some resistance as seen in Fig. 3b; the ten ohm curve shows this drastically changed curve.

The series and shunt resistance both affect the characteristics. The shunt, as seen in Fig. 4, shows that below 100 ohms the effect is great; but, above it, the effect is minor. The shunt resistance is due to the junction edge and crystalline faults that show up after sintering of the contacts due to the contact metal diffusing down microcracks into the junction. Except for low current densities, the shunt resistance can be neglected. The series resistance is the dominate loss and will be discussed later in this chapter.

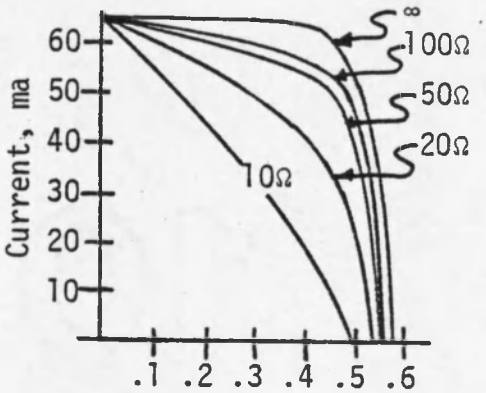

Fig. 4. The Effect of the Shunt Resistance on the Solar Cell with the Curve Shifted from the Fourth to the First Quadrant.

The junction is not ideal and the curve is modified by a factor in the exponential. The results of the testing so far indicates that the term m in the expression:

$$I = I_o \left(e^{\frac{q(V-IRS)}{mKT}} - 1\right) - I_L \qquad (4)$$

is equal to 1.1744 for the 2 cm x 2 cm, 1 Ω-cm wafer. With the value of I_o equal to 4.069×10^{-10} amp for the new photovoltaic model.

The resulting value of m gives an effect on the curve fill factor for the wafer as seen in Fig. 5.

$$CFF = V_M I_M / V_{oc} I_{sc} \tag{5}$$

V_M and I_M are the maximum power points for the voltage and current.

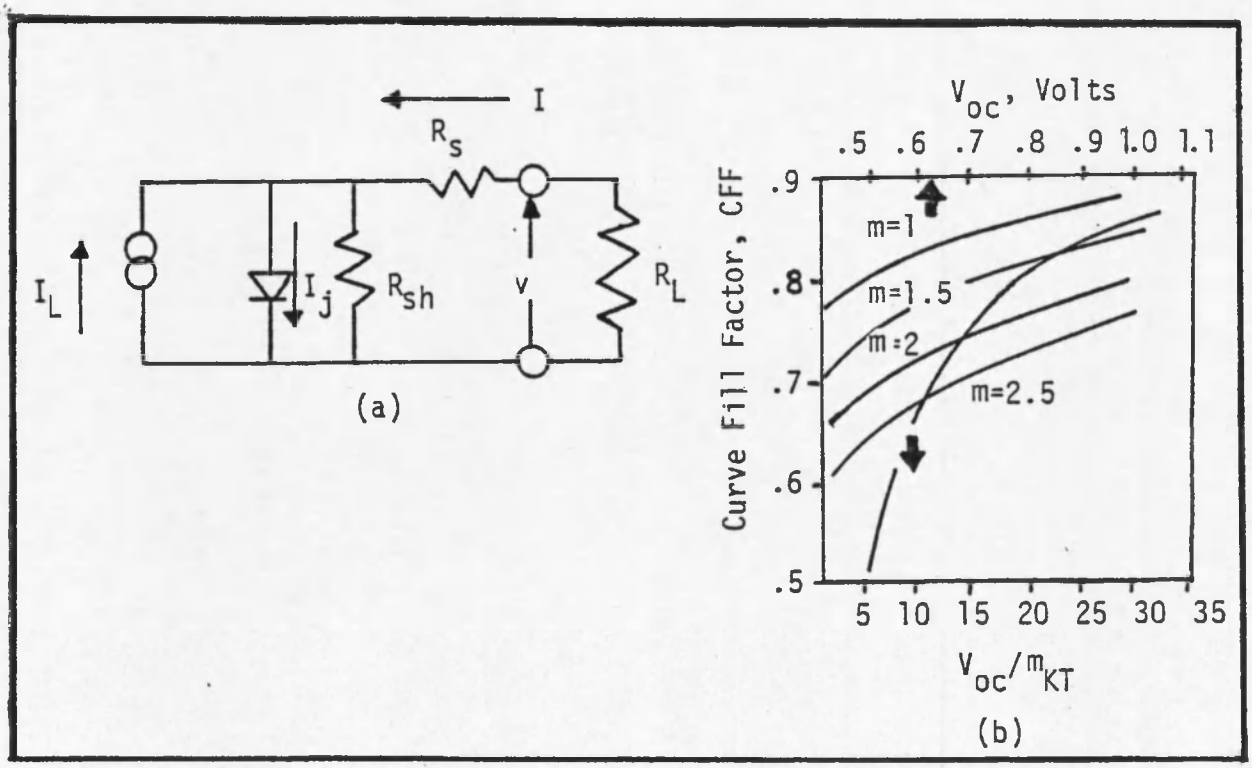

Fig. 5. (a) Real Solar Cell Model; (b) Curve Fill Factor as a Function of Normalized Open-circuit Voltage, Valid for all V_{oc}, m, and T.

Also shown are four curves for m = 1 - 2.5 at 298°K.

So with the value of M close to one, we see that V_{oc} = .58v; the CFF is 0.82. Experimentally, the value at 100 mw/cm^2 was 0.82 for the CFF.

The shape of the curve is important. This shape is the relative value of the power and efficiency that can be gotten out at the maximum power point. The effect of small resistances is detrimental to the efficiency of a cell. For example, if a wafer was under concentration of 20 suns (2 w/cm^2) and had a series resistance of one ohm, the wafer would lose 0.5v or about a loss of 84 percent of the power per square centimeter. So small values of resistance acceptable in the first space solar cells are unacceptable for concentration solar cells.

The Efficiency of a Cell

Solving equation number two for the maximum theoretical efficiency, we get this expression:[4]

$$N_{MAX} = \frac{V_M I_M}{\text{Power-IN w/cm}^2} = \frac{(q\ V_M/mKT)\ |1 + I_o/I_L|\ |I_L|\ V_M}{(1 + q\ V_M/mKT)(N_{ph}E_{av})\ A} \qquad (6)$$

Where N_{MAX} is the maximum efficiency, N_{ph} is the average number of photons of energy greater than the bandgap energy.[5] The value of I_o is equation (1) divided by (exp(q V/KT) - 1)

---

4. S. M. Sze, Physics of Semiconductors, John Wiley and Sons, Interscience, New York, 1969, p. 649.

5. S. W. Angrist, Direct Energy Conversion, Allyn and Bacon, Second Edition, Boston, 1971, p. 189.

Table 1. Solar Flux with Atmosphere Mass Numbers*

Mass Number	Water Content	Comments	Φ (w/cm^2)	E_{av} (ev)	N_{ph} (No/sec-cm^2)
0	0	Outside Atmosphere	0.135	1.48	5.7×10^{17}
1	0	Sea Level, Sun at Zenith	0.106	1.32	5×10^{17}
2	0	Sea Level, Sun at 60 Degrees from Zenith	0.088	1.28	4.3×10^{17}
3	0	Sea Level, Sun at 70.5 Degrees from Zenith	0.075	1.21	3.9×10^{17}
1	2	About 50% Relative Humidity	0.103	1.25	4.8×10^{17}
3	5	Extreme Condition	0.054	1.18	3.2×10^{17}
1	0	Cloudy Day (7000^{o}K Black Body)	0.012	1.44	5.2×10^{16}

*Angrist, 1971, p. 190.

Since the value will be less than the maximum, the equation can still be used for measured values of I_M and V_M. To get the theoretical I_M and V_M, use iterative techniques to solve for the value of each.

$$I_M = \frac{-(I_L + I_o)\, q\, V_M/mKT}{1 + q\, V_M/mKT} \tag{7}$$

$$V_M = mKT/q \ln \left(\frac{I_M + I_L + I_o}{I_o}\right) \tag{8}$$

Constant Illumination and Variable Temperature

Solving the current equation for the exponential's power you get:

$$\ln\left(\frac{I + I_L}{I_o} - \left(\frac{V - IR_s}{I_o R_{sh}}\right) + 1\right) = q/mKT\ (V - IR_s) \qquad (9)$$

which shows the voltage is linear with respect to temperature decrease. This decrease in open circuit voltage is due to the strongly increasing dark current. The voltage decreases by -2.2mV/^{o}C for one ohm centimeter wafers.

The photocurrent increases slightly with increasing temperature, partly due to the improvement in the base diffusion length and partly due to the shift of the absorption edge to lower energies, both of which improve the long wavelength spectral response.[6] The amount that the photocurrent changes is only 0.02 - 0.08%/^{o}K or on a 25 ma cell 5 μa - 20 μa/^{o}K. This change is minor over a 25^{o}C to 50^{o}C change of temperature. The lifetime will be approximately constant in the temperature range in which the solar energy conversion will be considered with a doping level of 10^{17} per cm^3.

The coefficient I_o increases exponentially with temperature resulting in an exponential increase in Ij. This results in a linear decrease in the open circuit voltage.[7]

The careful measure of T. J. Faith[8] resulted in the values for change in photocurrent of 0.065 ma/^{o}K for 2Ω-cm wafers with an electron

---

6. Harold J. Hovel, Semiconductors and Semimetals: Solar Cells, Academic Press, New York, 1975, pp. 168-169.

7. Joseph J. Wysocki and Paul Rappaport, RCA Laboratories, "Effect of Temperature on Photovoltaic Solar Energy Conversion," Journal Applied Physics, Vol. 31, March 1960, pp. 571-578.

8. T. J. Faith and A. F. Obenschain, "Temperature, Illumination, and Fluence Dependence of Current and Voltage in Electron Irradiated Solar Cells," NAS-5-21642, U. S. Goverment Printing Office, Washington, D. C.

flux of 10^{13} to 10^{16} e/cm^2. The experimental error was ±1.4% for the light current measurement of the light flux from 5 mw/cm^2 to 1830 mw/cm^2.

The results between the papers show a +2.56% to +4% per 50°C change is noticed in the photocurrent. The change remained the same over the large flux changes in the data.

While the major lost in gaining temperature is due to the loss in voltage, the loss in voltage over 50°C is -16.9%. This results in a net loss in the power of -.287%/°C which decreases the efficiency. The loss in efficiency due to temperature of the wafers I fabricated was -.3575%/°C.

The symbols used for measurement of the parameters is shown in Fig. 6.

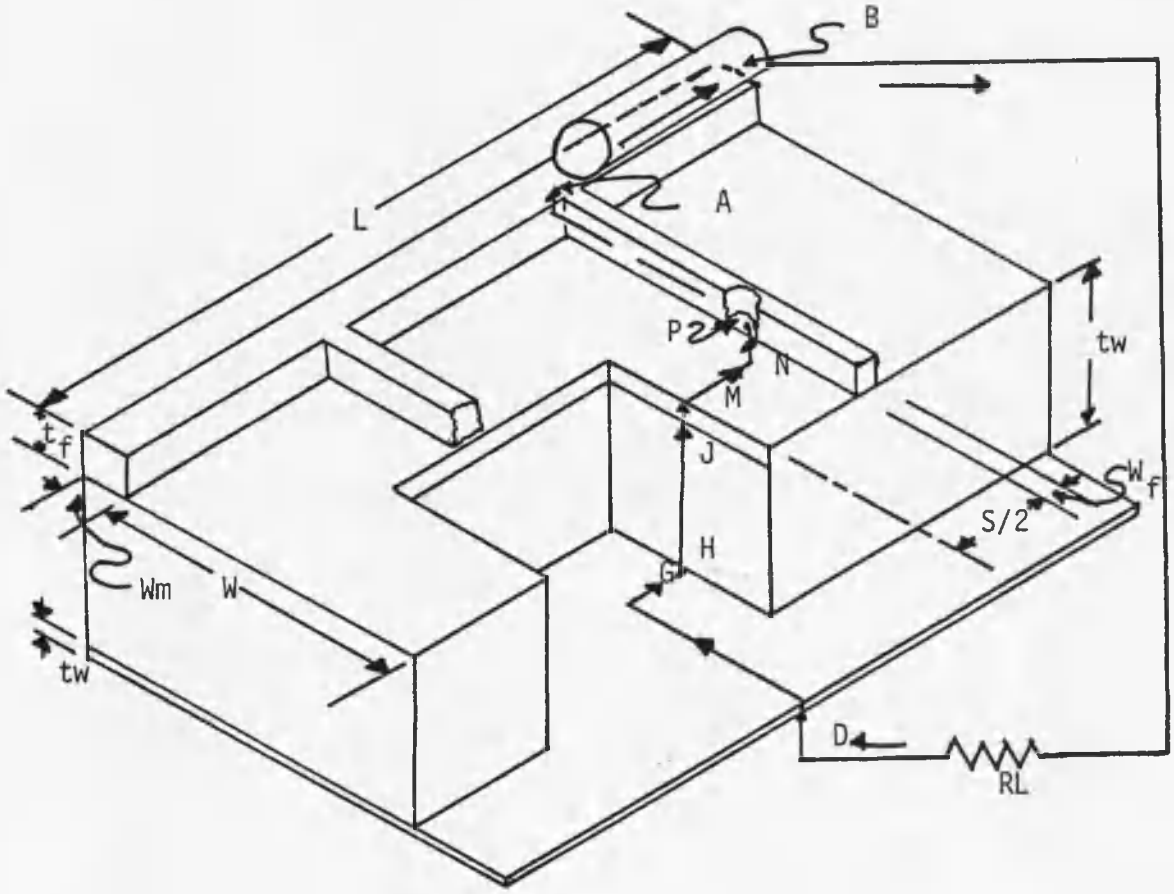

Fig. 6. The Losses Due to Resistance.

Points	Loss
M-N	V_L is due to the lateral resistivity and distance from the junction.
N-P	V_{ct} is due to the contact resistance at the metal-semiconductor interface at the top metal connections.
P-A	V_f is due to the finger resistivity.
A-B	V_m is due to the pattern and wire combination of the main.
B-D	V_{OUT} is the voltage the load sees.
D-G	V_{MB} is due to resistivity of the metal and solder of the back contact.
G-H	V_c is due to the contact resistance of the metal-semiconductor at the back.
H-J	V_b is due to the resistivity of the semiconductor to the bottom of the junction.

The Lateral Voltage Drop

The photon has created a hole electron pair and the junction has preferentially separated the carriers. To recombine the electron must travel the exterior loop to recombine at the back of the depletion region with a hole. First the electron seeks the shortest path to the contact grid. From the junction to the grid it sees a distance of, on the average, only 1/4 $(W_f + S)$ neglecting the junction depth.

The resistance is:

$$R_L = (W_f + S)\, \rho_L / 4W \tag{10}$$

where W_f is the width of the fingers, S is the field width, W is the length of the field, and ρ_L is the lateral resistivity and was 20Ω/□ for the process I ran.

The resulting voltage drop is:

$$V_L = F\, (S + W_f)^2\, \rho_L / 8 \tag{11}$$

and substituting $1/N_f$ for $S + W_f$, we get:

$$VL = F\rho_L / 8N_f^2 \tag{12}$$

which is the approximation for the loss that we will use.

The Ohmic Metal-semiconductor Interface

The constant was determined experimentally and is only an approximation with the respect of area top and bottom and not a current

through the N^+-type to metal layer, since this value was determined using 0.01 ohm-cm N-type bulk experimentally.

The measured values were corrected for metal and the 0.01Ω-cm wafer bulk resistance. Working backwards from the measured increase, the results indicate that the high doping of 8.5×10^{20} atoms/cm^3 provides a low contact resistance to the front contact. The values measured are only approximate (Table 2):

Table 2. Contact Resistance.

Rc(TiAg)	= 0.0076Ω-cm^2 for 100-200 Å Ti, 1200 Å Ag
Rc(TiPdAg)	= 0.022435Ω-cm^2 for 400 Å Ti, 200 Å Pd, 1200 Å Ag

Assuming that the front contact provides no contact resistance, the ohmic loss is from the back.

$$R_{con} = \frac{R_c\ (TiAg)}{A_S} \tag{13}$$

The value of the term A_S is the back contact area. The voltage loss:

$$V_c = F\ (A_F)\ R_{con} \tag{14}$$

where A_F is the area of the front of the cell. Since F is normalized to the cell, with the contact pattern already shadowing the percentage of area. The value of F is experimentally determined at close to 25 ma/cm^2 with ten percent of the area shadowed.

This gives for Vc after dividing out the areas since $A_F = A_S$ in most cells.

$$V_c = FRc\ (TiAg) \tag{15}$$

This shows that the voltage loss is directly related to the input light intensity.

The Thin Metal Finger

The loss as the electron travels down the thin metal finger is a resistive loss.

The resistivity of the contacts is given below for the two contacts used and values of the measured semiconductor-metal interface is given in Table 3.

Table 3. Contact Material Resistance.

ρ_f	Composition
$1.38 \times 10^{-3}\ \Omega/\square$	400 Å of Ti, 200 Å of Pd, 1200 Å Ag, 12 μm Cu
$1.276 \times 10^{-3}\ \Omega/\square$	100 Å of Ti, 1200 Å of Ag, 12 μm Cu

The current adds up as the current travels to the main. This results in the length looking half as long.

The equation:

$$V_f = \frac{FW^2\rho_F S}{2W_f t_f} \tag{16}$$

is the voltage drop down the finger at the main. The term ρ_F is the resistivity of the metal and when divided by the thickness, t_f, the result is ρ_f given above. The terms W_f/S is the fraction of light blocked by the fingers and we will call this α.

The resulting equation:

$$V_f = \frac{FW^2\rho_f}{2\alpha} \tag{17}$$

gives the voltage drop with the estimated allowable coverage of area by the finger pattern.

The Loss on the Main

The current soon adds up to a sizable value causing a large voltage drop down the metal fingers. So a main is put on the cell to get the current out with as little loss as possible. The main has a soldered wire on it to cut the loss even more.

Let us first consider a main of the same material as the fingers of 20 mils wide (W_m) under a concentration of 100 suns, so F = 2.5 amps/cm^2, and a length of 2 cm (L) and one outlet for the current.

The equation:

$$V_m = \frac{\rho_f FWL^2}{W_m} \tag{18}$$

for the main with two equal fields on each side. If we plug in values, we get V_m = .25v. This value is much too high so a wire is soldered to the main. The equation (with $W = W_m$):

$$V_m = \frac{F}{(NC)}(WL)\frac{(\rho_f\rho_m L^2/W_m)}{(\rho_f L/W_m + \rho_m L)} \tag{19}$$

is the final voltage drop down the main. The term NC is the number of points that you take the power from the main. It can be either one

or two. If the take off is a strip, then the resistance of the strip is divided by the area. For example:

$$V_m = FWL \left(\frac{W_m}{L} \rho_f + \frac{\rho_{cu}}{t_s} \frac{W_S}{L}\right)$$

$$\rho_{cu} = 1.7 \times 10^{-6} \Omega\text{-cm} \qquad (20)$$

this gives a very low series resistance for cell interconnection. W_S is the width of the copper strip. The values of the wire resistance used is given in Table 4.

Table 4. Wire Resistivity Table.

ρ_m ohm per/cm	Wire Size	Width Main Needed
3.723×10^{-4}	#20	40 mils
4.416×10^{-4}	#24	30 mils
1.5×10^{-4}	#26	20 mils

The Ohmic Loss in the Metal Back Contact

The metal on the back with solder on top of it will have an average resistivity of the two.

$$\rho_{solder} = 16 \times 10^{-6} \Omega\text{-cm}$$

$$\rho_{cu} = 1.7 \times 10^{-6} \Omega\text{-cm}$$

When a wafer is solder dipped, you pick up about 20 μm of solder on the back contact. The result is the same as approximately on μm of copper.

The equation (for rectangular cells):

$$V_{MB} = F(2L\ (W + W_m/2))\ \frac{\left(\frac{\rho_{cu}}{tcu}\ \frac{L}{2(W + W_m/2)}\ \frac{\rho_{solder}\ L}{t_{solder}(2W + W_m)}\right)}{\frac{L}{2W + W_m}\ \left(\frac{\rho_{cu}}{t_{cu}} + \frac{\rho_{solder}}{t_{solder}}\right)} \qquad (21)$$

The equation (for square wafers):

$$V_{MB} = FL^2\ \frac{(\rho_f)}{\frac{\rho_f}{\left(\frac{\rho_{solder}}{t_{solder}}\right)} + 1} \simeq FL^2\ \frac{\rho_f}{1.174} \qquad (22)$$

and the value for ρ_f is the sheet resistance of the metal contact before solder.

The Bulk Resistance

The bulk resistivity is a function of the doping. The decrease in resistance of a factor of ten from 10Ω-cm decreases the photocurrent about four percent and increases the open-circuit voltage by 0.03 volts. So, if we go down in resistivity, we see an increase in efficiency due to the voltage increase and can add $\Delta I L \Delta R_s^2$ gain to the power.

Considering the bulk resistance, R_b, and the voltage drop we have:

$$R_b = \rho_b\ t_w/A_F \qquad (23)$$

where ρ_b is the resistivity of the bulk wafer, t_w is the thickness

of the wafer, with the junction depth neglected, and A_F is the surface area of the front side of the wafer.

Now,

$$V_b = IR_b \tag{24}$$

where V_b is the voltage drop across the bulk wafer and I is the total current carried by the cell. So

$$V_b = \rho_b t_w I/A_F \tag{25}$$

but I/A_F is the current per unit area and is approximately F.

$$V_b = F\rho_b t_w \tag{26}$$

So notice no dependence on the size of the wafer for the voltage loss due to the bulk, but only on its thickness and resistivity.

Using these equations, cells were designed to minimize as many of the voltage drops as possible. The design was not an optimization but an attempt to minimize internal resistance. Many trade offs are available, such as increasing the number of fingers and changing the finger width to 86 percent of the previous value, you decrease the amount of light hitting the wafer but maintain a higher curve factor longer. The result is a cell that has lower efficiency at the lower suns than the previous pattern, but higher amounts of power out as the upper limit is reached. The next chapter will discuss some of the patterns tested and the results.

CHAPTER 4

RESISTANCE MEASUREMENTS OF A SOLAR CELL

The test patterns were of different designs. The experimental data on the different finger patterns gave data on the areas of control. These areas are the finger width, density, and placement of the mains. Cells with finger densities (N_t finger/cm) of 30, 22.5, 15, and 10 were fabricated and tested. In Appendix A, Tables 5 through 16, each pattern is tabulated for the voltage drop for each part of the cells. The method used for the measurement of the resistance was first used by Wolf, and this method is presented in Appendix B with the model shown in Fig. 8, with a check on the accuracy of this method. A detailed report on the fabrication process in given in Appendix C. The curves (Figs. 9 through 21) and listings of the values (Tables 17 through 22), are illustrated and tabulated in Appendix D.

The wafer material for the 2m x 2 cm test wafers was P-type 1Ω-cm single-crystal Silicon of a thickness 0.033 cm (tw). The 10 finger/cm pattern (Pattern F, Table 22, Fig. 21) was a two-inch wafer of 3Ω-cm material and was scribed into two flat sides for eventual mounting as a one-unit of four cells forming a cloverleaf pattern.

This cloverleaf design was designed for an efficiency of 10 percent at ten suns. The wafers were tested at 55°C and gave an efficiency of 10.3 percent at ten suns.

The test patterns A, B, and D which have a N_t of 22.5, 30, and 15 have dimensions in common. The main contact has a width of 0.0508 cm and length of 2 cm.

The finger length was 0.9746 cm, and a junction depth for all patterns was a phosphorus diffusion of 0.4 μm and a sheet resistance (ρ_L) of 20Ω/□. The 3Ω-cm wafer had a junction of approximately 0.4 μm and a sheet resistance of 20Ω/□. The metal contacts were of titanium and silver with a copper plate of 12 μm. The contact was put on in a vacuum station and was photoresisted and etched into the particular pattern.

The present cost of solar cells is high. With the use of concentrators, the cost per peak watt can be cut, if the efficiency does not drop. The cost per watt is then the cost of the tracking system, concentrator, and solar cells divided by the number of peak watts. The usable range for concentration of the cells for reasonable cost to return is the increase in suns to where the efficiency has dropped to eight percent on the cells. This means the cells can be usable to 100 suns. So let's look at the losses in Pattern A at 100 suns.

The pattern losses for a total contact area of 10.89 percent for Pattern A is as follows:

V_b = 0.0825 v	Loss due to the Bulk Resistivity
V_L^b = 0.0123 v	Loss due to the Lateral Resistivity
V_f^L = 0.01847v	Loss due to the Metal Resistivity
V_c^f = 0.0190 v	Loss due to Metal-Semiconductor Interface
V_m^c = 0.01425v	Loss due to Power taken from Two Ends of Cell
V_{MB} = 0.0124 v	Loss due to Metal
V_t = 0.1599 v	

We noticed that the major loss is in the bulk. To reduce this loss, the solar cells can be fabricated with lower resistivity. This would reduce the lifetime of the minority carriers. The current will decrease slightly but the open circuit voltage will increase. The result in going down to a 0.1Ω-cm is theoretically a higher efficiency under concentration.

This concentration results in a linear light current increase and the voltage increases in a logrithmic fashion so the lowering of the resistance is a paramount function. So let's use the data for the curve fill factor.

The equation:

$$CFF = \frac{V_M I_M}{I_{sc} V_{oc}} \tag{27}$$

is the curve fill factor equation with V_M and I_M being the maximum power voltage and current points.

The test patterns were of different finger densities and widths. The three patterns were chosen with different ratios of α (α is equal to the width of the finger divided by the field width) such that the voltage drop down the fingers remains similar. The drop at 100 suns light flux for Pattern B (30 fingers/cm, one main) is 0.0158v. The Pattern A (22.5 fingers/cm) is 0.0185v, and Pattern D (15 fingers/cm) is 0.0164 volts. The difference is smaller than the lateral resistivity so this part of the design forces the difference in the lateral resistivity to be more prevailing than the other losses.

The comparison of the voltage losses shows that values of the losses for the bulk and contact resistance, the main, and the back metal contact of Patterns A, B, and D to be equal. This leaves the contact resistance and the lateral resistance, the latter as the remaining variable. This means that the variable of the lateral resistance will show the greatest change in the curve fill factor. The plot of the CFF on Illustration 9 shows the differences. Since Pattern A has the least area covered, it gave the highest efficiency of the test patterns.

To check this, the pattern for the cloverleaf was designed with this in mind. The comparison of the high efficiencies at 100 mw/cm^2 can be made. The cloverleaf has reached a high of 12.05 percent with a current density of 26.38 ma/cm^2 exposed area is 90.6 percent of wafer. Correcting for area, this wafer has an efficiency per exposed area of 13.3 percent. The current density is 29.117 ma/cm^2 for the exposed silicon on the cell. The maximum efficiency of Pattern A with a .4 μm junction was 11.6 percent at one sun and a current density of 23.2 ma/cm^2 for an exposed area of 89.11 percent, so a final efficiency of 13.02 percent and a corrected area current density of 26 ma/cm^2.

The best to date is a 12.2 percent actual, 13.69 percent area corrected solar cell with a shallow junction and sheet resistance of 86Ω/□. The current density was 26.25 ma/cm^2 uncorrected and 29.45 ma/cm^2 area corrected. This compares with the cloverleaf and indicates the decrease in lifetime from the 3Ω to the 1Ω is not that big since the junction depth of the shallow junction is of the range of .22 to

.4 μm so the difference is the base lifetime and the diffused junction lifetime.

Comparing the CFF pattern for the 0.4 μm junction test wafers at 30 suns, we find that Pattern B is the best with 0.79. A is next with 0.74, and Pattern D was the lowest at 0.695. These compare with the direction that the lateral voltage drop increases. The indication is that the closer your fingers are, the lateral resistance drops; but, as you get closer, the fingers must thin and then the state of the art comes in to limit the design.

The number of mains is also a factor in the CFF. The net result is that a lot of mains do what a lot of fingers do at high intensities. Looking at Fig. 9, page 51, we notice that Pattern E crossed Pattern A at 40 suns. At that point, the 4 cm^2 cell of Pattern E has .87 amps/cm^2 while Pattern A has .93 amps/cm^2, since the voltage loss divided by the current out is approximately the resistance we see. Then solving for the total voltage loss of Pattern A and E, we get V_E = 0.075 V_A = 0.081 4v, R_E = 0.0214Ω, and R_A = 0.0218Ω. This shows experimentally the crossover point of shortening the effective length of the finger can reduce it sufficiently to counter the lateral voltage drop. However, the loss at low intensities because of the magnitude of the lateral drop shows the CFF of E to follow D to where the intensity is such that Pattern D loses power more rapidly. The theoretical V_t shows that Pattern E is 0.007v better, and shows that the loss is due to the junction seeing a high voltage at the center of the field until the current density gets such that Pattern A has lost the same

amount of power. The match up of theoretical loss of 0.007v to an actual differential 0.006v is small. Since the test apparatus had 0.007 - 0.011Ω inherent in it due to the resistivity of #6 wires running from the mount to the test stand and the connecting lengths of #26 wire, the results were corrected at each hookup.

The effective efficiency increases as the light intensity increases because the photocurrent and voltage increase. The area minimization for the contact pattern is the greatest concern for high intensity use. Main contacts are area gobblers; but, in order to get low resistance, a wire must be soldered which means the main must be of the same size as the wire. The result is a cell with low resistance, if it was zero there would be an increase in efficiency as intensity increased if the cell was held at a constant temperature.

The real result is that the photocurrent is increasing linearly with the light intensity but the power loss is increasing by the square of the photocurrent. The result is a loss in efficiency. The loss increases as the temperature increases because of the negative thermal coefficient for the voltage. This has been seen to occur at high light fluxes of 150x where the open-circuit voltage is below the voltage of a lower light flux of 125x. Shadowing of the cell and then quickly measuring shows the temperature dependence. The gains at lower intensities are not totally seen to be cancelled by the losses.

The result is a peaking of the efficiency. This has been observed to occur for Patterns A, B, and C at about ten suns. The increase is about ten percent of the original efficiency.

This peaking allows a design flexibility where intensity at use can be almost the same as the one sun room temperature value. Since both the cooling and resistive losses present problems, the ability to design for a wide range of intensities such that as the day passes the unit would be as efficient as the mid-peak due to the different light fluxes and temperatures would be desirable.

The design of a passive air-cooled system was done. Considered for the design was the process variations, temperatures, and light fluxes. The design called for ten percent efficiency with the cells at $55^{o}C$. The wafers were fabricated for this cloverleaf pattern using ten fingers/cm and 3Ω-cm material.

The mask was designed to give these specifications. Four wafers were fabricated and then mounted with epoxy to an aluminum plate. Then they were tested at $55^{o}C$ and found to have an efficiency at ten suns of 10.3 percent and a resistance of 0.0240Ω which is acceptable at 4.7 amps photocurrent. The theoretical resistance is 0.013Ω.

So, in designing a solar cell, the resistance can be limited. The resistance of Pattern A was found to be 0.016Ω, Pattern B was 0.0155Ω, Pattern C was 0.0141Ω, Pattern D was 0.018Ω, and Pattern E was 0.014Ω. The experimental results compare favorably with the theoretical calculated values.

These results show that the model is a good approximation for a high intensity solar cell.

CHAPTER 5

CONCLUSION

The factors that cause the resistance can be limited. Losses due to the lateral resistance no longer have to be the controlling limit for a solar cell. The new limit is getting low resistance bus bars that can handle fourty amps from a large number of sub-arrays. Units from 0.5 cm^2 to 65 cm^2 have been made in the Solid State Laboratory by myself.

One experimental test involved a multiple junction cell. The cell performed well under concentration. The area was 2 cm x 1 cm with a V_{oc} of 7.25v and I_{sc} of 5 ma. This experiment showed that high voltages can be supplied at low currents with small area.

The test result of a seven-cell array of 2 cm x 2 cm wafers in series showed the usable power is sufficient to lift 500 grams one meter in three seconds with a light flux of one sun.

The technology is here and the power can be used for less cost than cells designed for use at one sun. This means that concentration is one way to cut the cost of photovoltaic systems. The concentration solar cell uses low cost fuel which will be here a lot longer than I will. The savings in fuel could be enough that the system not only pays for itself but gives a capability for growth.

APPENDIX A

VOLTAGE LOSSES FOR EACH PATTERN

In Tables 5 through 16, the common parameters and tabulated values of each pattern is found.

Table 5. Contact Pattern Data.

Pattern	No. of Fingers/cm	No. of Mains	Total Pattern Change
A	22.5	1	10.89
B	30.0	1	12.19
C	30.0	2	19.46
D	15.0	1	11.82
E	15.0	3	16.40
F	10.0	2	9.4

Table 6. Finger, Mains Widths.

	Finger Width (W_f)		Main Contact Width (W_m)		Ratio of Width of Field to Finger Width (α)
Pattern	mils	10^{-4} x cm	mils	10^{-4} x cm	
A	1.5	38.1	20	508.0	0.09376
B	1.3	33.0	20	508.0	0.110
C	2.0	50.8	20	508.0	0.180
D	2.5	63.5	20	508.0	0.105
E	2.5	63.5	20	508.0	0.105
F	2.3	58.4	30	762.0	0.062

Table 7. Area of Coverage.

Pattern	Percentage of Total Area for the Main	Percentage of Total Area for the Fingers
A	2.54	8.35
B	2.54	9.65
C	5.08	14.47
D	2.54	9.28
E	7.6	8.799
F	4.0	5.37

Table 8. Shape.

Pattern	Pattern Shape	Junction Depth (μm)	Sheet Resistance Ω/□
A	2 x 2 cm	0.4	20
B	2 x 2 cm	0.4	20
C	2 x 2 cm	0.4	20
D	2 x 2 cm	0.4	20
E	2 x 2 cm	0.4	20
F	Chopped 5.08 cm round with two sides perpendicular to each other	0.4	20

Table 9. Length and Width.

Pattern	Length of Main (cm) (L)	Spacing of Mains	
		From Each Other (cm)	From Edge (cm)
A	2	--	0.9746
B	2	--	0.9746
C	2	0.95	0.475
D	2	--	0.9746
E	2	0.308	0.308
F	4.36	2.00	1.09

Table 10. Common Parameters.

α	=	$W_F/(\frac{1}{N_f} - W_F) \simeq 0.105$
t_{cu}	=	12×10^{-4} cm, Thickness of Copper Plate
ρ_L	=	20Ω/□, Sheet Resistance
ρ_F	=	1.7×10^{-6}Ω-cm, Average Contact Resistance
t_f	=	12.2×10^{-4}cm, Thickness Total of the Contact
ρ_f	=	1.393×10^{-3}Ω/□, Sheet Resistance of the Contact
t_w	=	0.033cm, Thickness of Wafer
W	=	0.9746cm, For Patterns A, B, D

Table 11. Pattern A--22.5 Fingers/cm.

$$V_b = 0.08250v = F\rho_b tw = 2.5 \times 1 \times 0.033$$

$$V_L = 0.01235v = \frac{F\rho_L}{8(N_f)^2} = \frac{2.5 \times 20}{8 \times (22.5)^2}$$

$$V_f = 0.01847v = \frac{F(W)^2\rho_f}{2\alpha} = \frac{2.5 \times (0.9746)^2 \times 1.459 \times 10^{-3}}{2\ (0.09376)}$$

$$V_c = 0.01900v = FRc\ (TiAg) = 2.5 \times 0.0076$$

$$V_m = 0.01425v = \frac{F(AT)}{Nc} \times \left(\frac{\rho_F \rho m\ (L)^2/Wm}{\rho_f L/Wm + \rho mL}\right)$$

$$V_m = \frac{2.5\ (4)}{2}\ \left(\frac{1.459 \times 10^{-3} \times 0.0015 \times (2)^2/0.0508}{1.459 \times 10^{-3} \times 2/0.0508 + 0.0015 \times 2}\right)$$

$$V_{MB} = 0.0124v = FA_B\ \left(\frac{\rho_f}{1.174}\right) = 2.5 \times 4\ \left(\frac{1.459 \times 10^{-3}}{1.174}\right)$$

$$V_T = 0.15897v$$

The assumptions are F = 2.5 amps/cm^2; the number of suns is 100; ρ_m = 0.0015Ω/cm; apparatus error +0.007Ω, and $\rho_f = 1.459 \times 10^{-3}\Omega/\square$.

The resistance measured 0.01611Ω while the theoretical resistance is 0.016Ω.

Table 12. Pattern B--30 Fingers/cm.

V_b	=	0.0825v
V_L	=	0.0069v
V_f	=	0.0158v
V_c	=	0.0190v
V_m	=	0.01425v
V_{MB}	=	0.01240v
V_T	=	0.15085v

The assumptions are that F = 2.5 amps/cm^2 at 100 suns; ρ_m = 0.0015/cm; $\rho_f = 1.459 \times 10^{-3}\Omega/\square$, and the apparatus error is +.0095Ω. The resistance is 0.0151Ω.

Table 13. Pattern C--30 Fingers/cm with 2 Mains.

V_b	=	0.0825v
V_L	=	0.0069v
V_f	=	0.0097v
V_c	=	0.0190v
V_m	=	0.0071v
V_{MB}	=	0.0124v
V_T	=	0.1376 v

The assumptions are that F = 2.5 amps/cm^2 at 100 suns; ρ_m = 0.0015Ω/cm; ρ_f = 1.459Ω/□, and the apparatus error is +0.0105Ω. The resistance measured is 0.0141Ω while the theoretical resistance is 0.0138Ω.

Table 14. Pattern D--15 Fingers/cm.

V_b	=	0.0825v
V_L	=	0.0278v
V_f	=	0.01637v
V_c	=	0.0190v
V_m	=	0.01425v
V_{MB}	=	0.0124v
V_T	=	0.17232v

The assumptions are that F = 2.5 amps/cm^2 at 100 suns; ρ_m = 0.0015Ω/cm; $\rho_f = 1.459 \times 10^{-3}$Ω/□, and the apparatus error is +.010Ω. The resistance measured is 0.0186Ω with the theoretical resistance being 0.017Ω.

Table 15. Pattern E--15 Fingers/cm with 3 Mains.

V_b	=	0.0825v
V_L	=	0.0278v
V_f	=	0.001635v
V_c	=	0.0190v
V_m	=	0.00475v
V_{MB}	=	0.0124v
V_T	=	0.148085v

The assumptions are that F = 2.5 amps/cm^2 at 100 suns; ρ_m = 0.0015Ω/cm; ρ_f = 1.459 x 10^{-3}Ω/□, and the apparatus error is +0.0105Ω. The value of resistance measured is 0.0148Ω and the theoretical resistance is 0.0148Ω.

Table 16. Pattern F--Cloverleaf Pattern.

$$V_b = 0.02858v = 0.25 \times 3 \times 0.0381$$

$$V_L = 0.00625v = \frac{0.25 \times 20}{8 \times (10)^2}$$

$$V_f = 0.00294v = \frac{0.25 \times (1)^2 \times 1.459 \times 10^{-3}}{2 \times 0.062}$$

$$V_m = 0.00868 = 0.25 \times (4.318 \times (2 + 0.0762))$$

$$V_c = 0.0019 = .25 \times 0.0076 \times \left(\frac{1.459 \times 10^{-3} \times 0.0094 \times \frac{(4.318)^2}{0.0762}}{1.459 \times 10^{-3} \times \frac{4.318}{0.0762} + 4.06 \times 10^{-3}}\right)$$

$$V_{MB} = 0.00511v = 0.25 \times 16.45 \left(\frac{1.459 \times 10^{-3}}{1.174}\right)$$

$$V_T = 0.05346$$

The assumptions are that F = 0.25 amps/cm^2 at 10 suns; ρ_b = 3Ω-cm; ρ_m = 0.00094 /cm; ρ_f = 1.459 x 10^{-3}Ω/□; tw = 0.0381cm and the apparatus error of +.00265.

The measured resistance was 0.024Ω. This is high because one of the wafers of the four had the resistance of the other three at one sun. The theoretical value is 0.013Ω.

APPENDIX B

THE DERIVATIONS OF THE EQUATIONS FOR EXPERIMENTALLY DETERMINING THE RESISTANCE

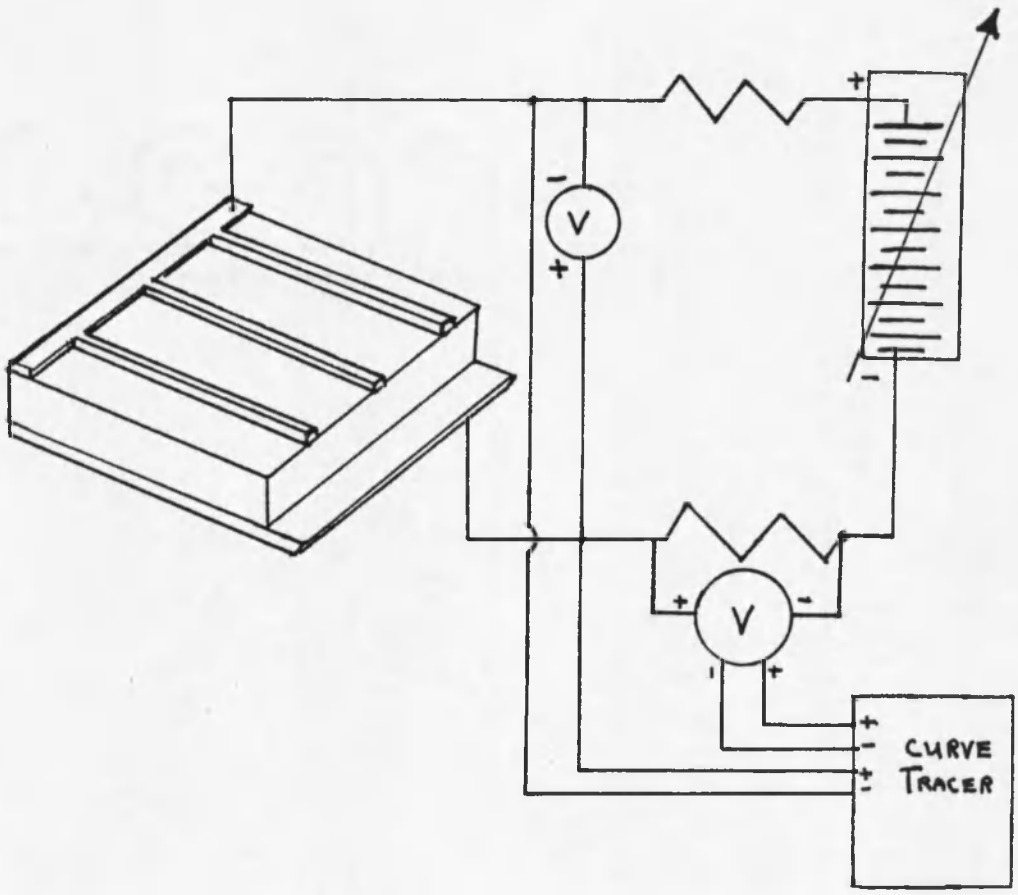

Fig. 7. Test Equipment Set Up.

Solar Cell Derivation of Resistance

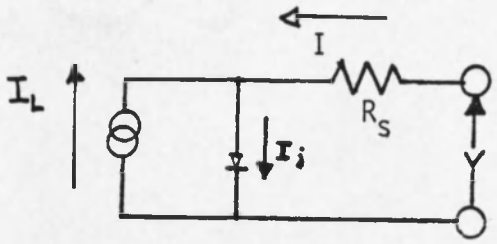

Fig. 8. Simplified Solar Cell Model.

Neglecting R_{sh}:

$$I = I_o \{e^{(q/AKT (V-IRS))} - 1\} - I_L$$

Let V'= V - IRS:

$$I = I_o (e^{BV} - 1) - I_L ; B = q/AKT$$

$$I_1 = I_o (e^{BV1} - 1) - I_{L1}$$

$$I_2 = I_o (e^{BV2} - 1) - I_{L2}$$

Setting $V_2 = V$; then let $I_{L2} = I_{L.} + \Delta I_L$ where ΔI_L is proportional to the difference in light intensity between levels 1 and 2.

When at high light levels $\Delta I_L >> I_o$.

V' = V - IRS is the voltage across the P-N junction. Note I is a negative quantity.

$$I = I_o (R^{B(V - IRS)} - 1) - I_L$$

$$I = I_o (e^{BV'} - 1) - I_L$$

$$I_1 = I_o(e^{BV'_1} - 1) - I_{L1}$$

$$I_2 = I_o (e^{BV'_2} - 1) - I_{L1} - \Delta I_L$$

Letting $V'_1 = V'_2$:

$$I_2 = I_1 - \Delta I_L$$

However,

$$V_1 - I_1R_s = V_2 - I_1R_s + \Delta I_L R_s$$

Thus a second translation of the axis gives different values at the terminals.

$$V_2 = V_1 - \Delta I_L R_s$$

So,

$$\frac{V_1 - V_2}{\Delta I_L} = R_s$$ or the slope of the line is the R_s.

The error of this method is discussed by Picciano and is as follows:[9]

$$\Delta R = \left|\frac{1}{I_2 - I_1}\right| (V_1 + V_2) + \left|\frac{V_1 - V_2}{(I_2 - I_1)^2}\right| (\Delta I_1 + \Delta I_2)$$

$I_{L1} = 6.6$ $\Delta V = .02v$

$I_{L2} = 4.5$ $I_{L3} = 2.85$

$I_1 = I_{L1} - \Delta I = 5.6$ $V_1 = .467$

$I_2 = I_{L2} - \Delta I = 3.48$ $V_2 = .550$

$I = 1$ amp I_3 $I_3 = 1.82$ $V_3 = .576$

---

9. Picciano, Wayne T., "Determination of the Solar Cell Equation, from Empirical Data," Energy Conversion, Vol. 9, Pergamon Press, Great Britain, 1969, pp. 1-6.

$\Delta V_S' = .3\%$

$\Delta I_S' = 1\%$

$$\Delta R = \left|\frac{1}{5.6 - 3.48}\right| \{.003 [(.467) + .53]\} + \left|\frac{.467 - .53}{(3.48 - 5.6)^2}\right|$$

$$[.01 (5.60) + .01 (3.18)] = 2.6838 \times 10^{-3}\Omega$$

APPENDIX C

THE FABRICATION PROCESS

Process Steps for Cell Fabrication

1. Cleaned wafers by scrubbing with acetone, isopropyl alcohol and de-ionized water using a Q-tip. Wafers were blown dry with dry N_2.
2. Diffused n layer by subjecting the wafer to a stream of $POCl_3$, carried by nitrogen, for fifteen minutes. Temperature at 912^oC.
3. Annealed wafer by pulling rapidly to 800^oC and pulling slowly to the end of the furnace.
4. Metallized the top with evaporative coatings of Ti-Ag.
5. Etch finger pattern into metal using standard photoresist technique.
6. Etched the n layer from the back using a Si etch. Top protected by coating of wax.
7. Metallize the back with Ti-Ag.
8. Etched edges of wafers to avoid shorts and leakage.
9. Copper plate both back contact and finger contact using $CuSO_4$ solution. Thickness of copper plate is 12 micrometers.
10. Solder main contact wire to center strip.
11. Test.

APPENDIX D

THE I-V, CFF, AND EFF CURVES FOR PATTERNS A THROUGH F

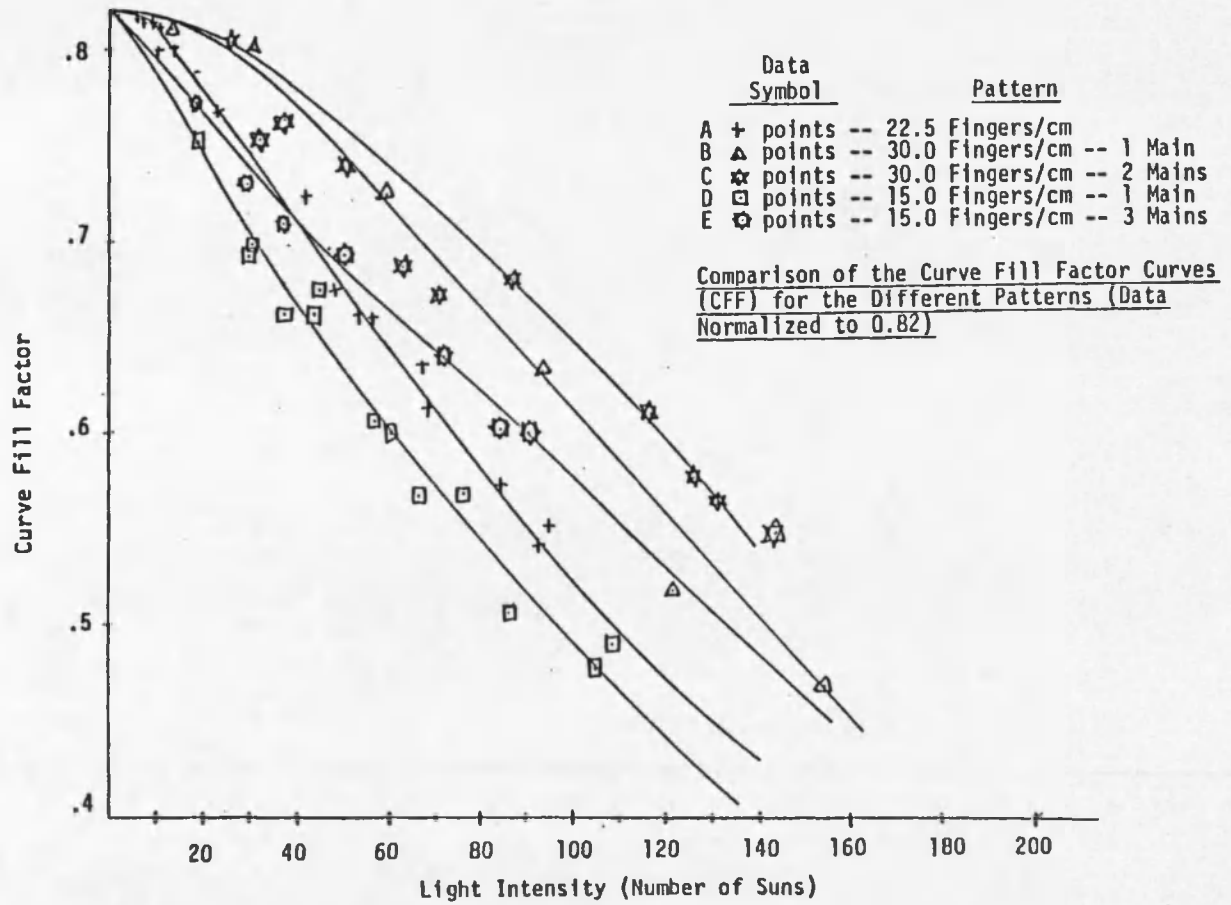

Fig. 9. Comparison of the Curve Fill Factor Curves (CFF) for the Different Patterns (Data Normalized to 0.82).

Table 17. Pattern A--Cell 17-12, 22.5 Fingers/cm.

Number of Suns	I_{sc}	V_{oc}	EFF	CFF
1	.095A	.57V	11.1	.82
2	.19	.59	11.4	.82
8.5	.8	.623	11.9	.82
38	3.5	.64	10.7	.71
68	6.5	.642	9.7	.64
84	7.9	.645	8.7	.57
159	15.0	.64	6.3	.41

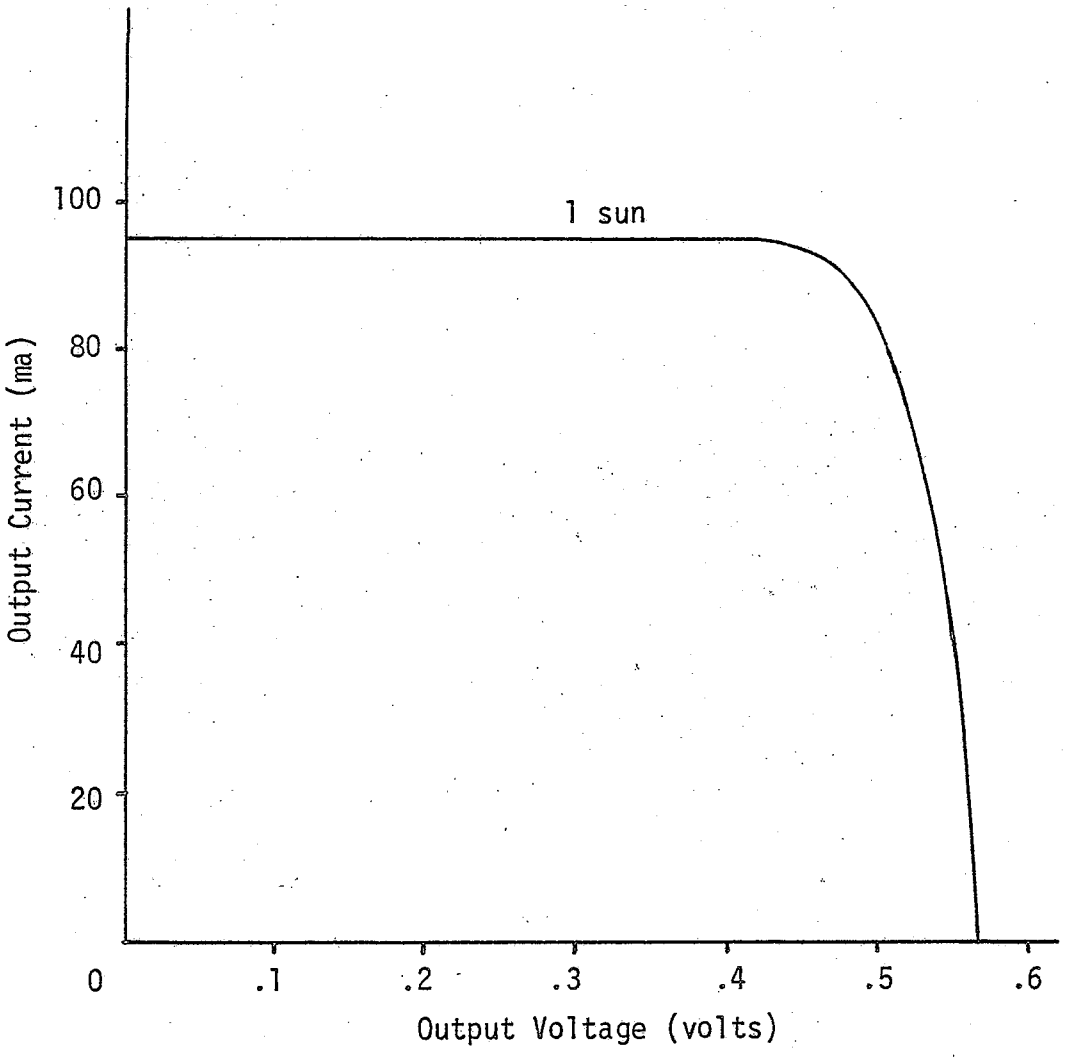

Fig. 10. Cell 17-12--22.5 Fingers/cm.

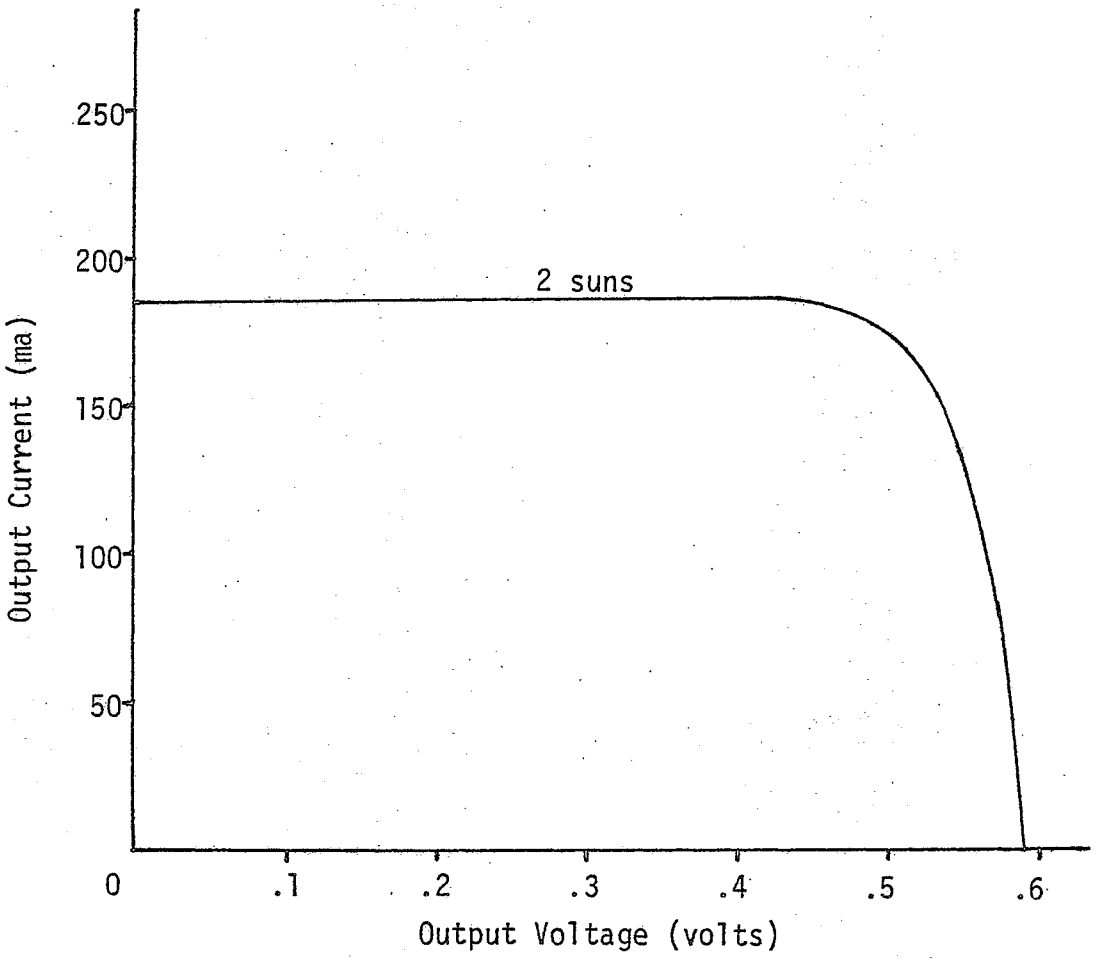

Fig. 10. Continued. Cell 17-12--22.5 Fingers/cm.

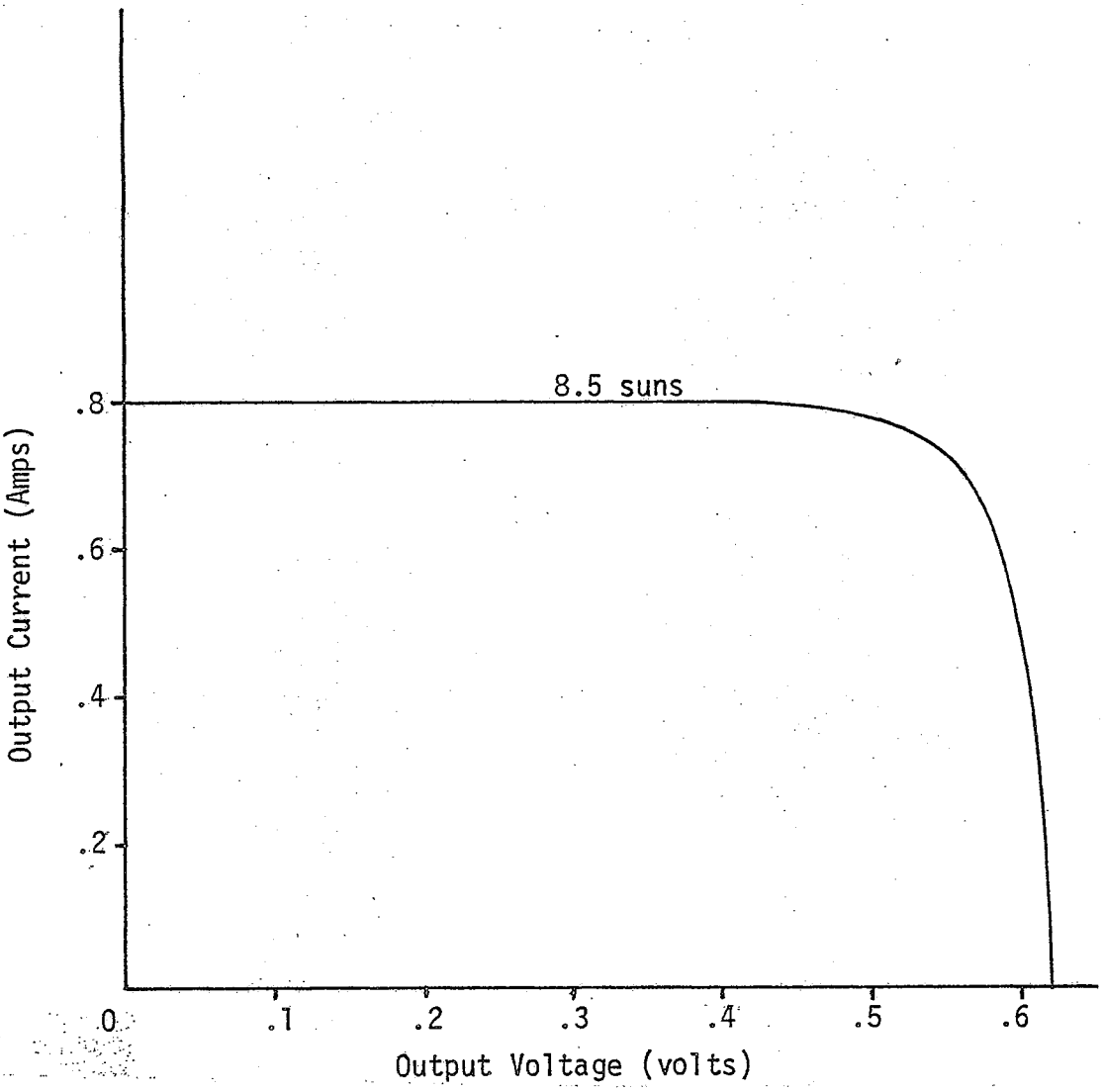

Fig. 10. Continued. Cell 17-12-22.5 Fingers/cm.

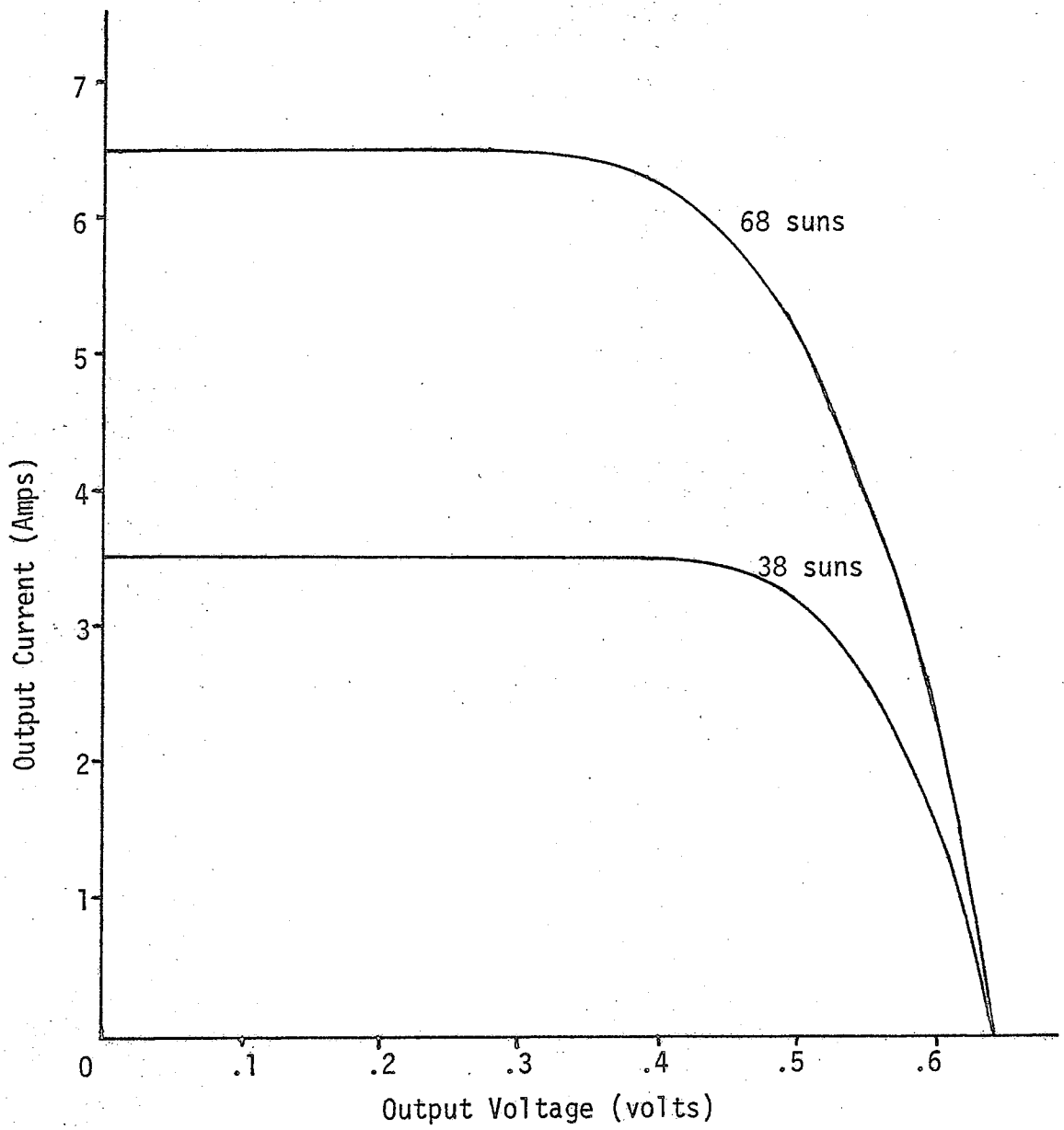

Fig. 10. Continued. Cell 17-12--22.5 Fingers/cm.

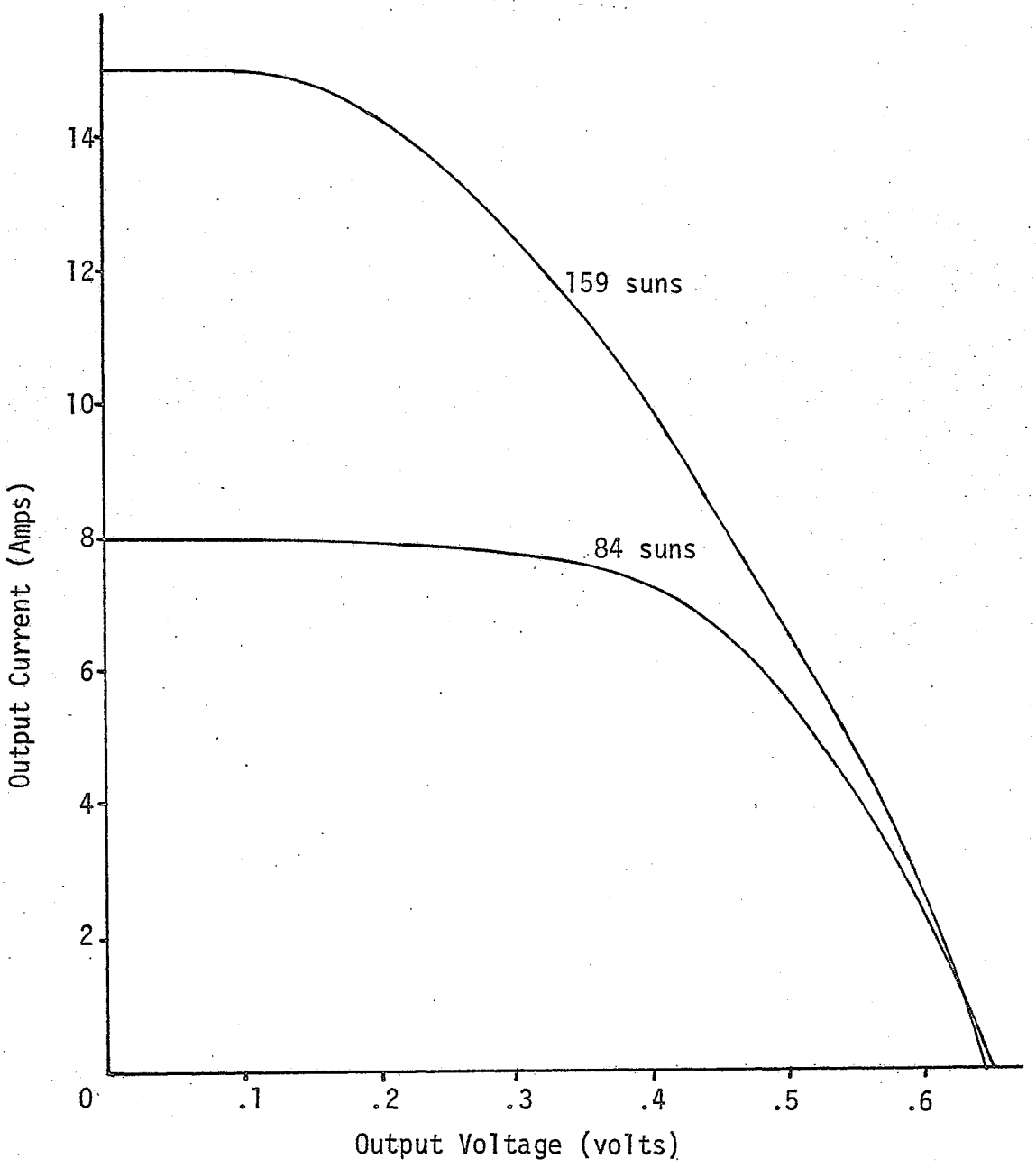

Fig. 10. Continued. Cell 17-12--22.5 Fingers/cm.

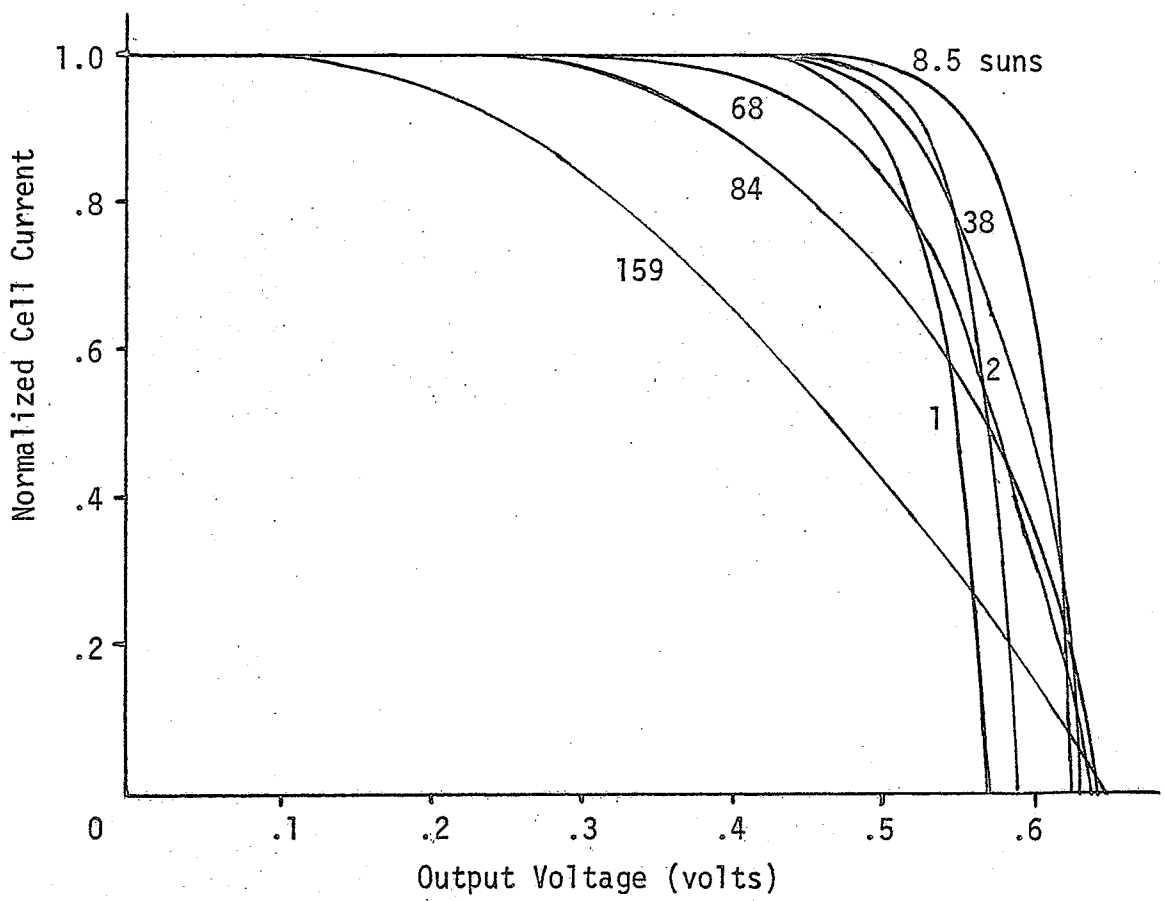

Fig. 10. Continued. Cell 17-12--22.5 Fingers/cm.

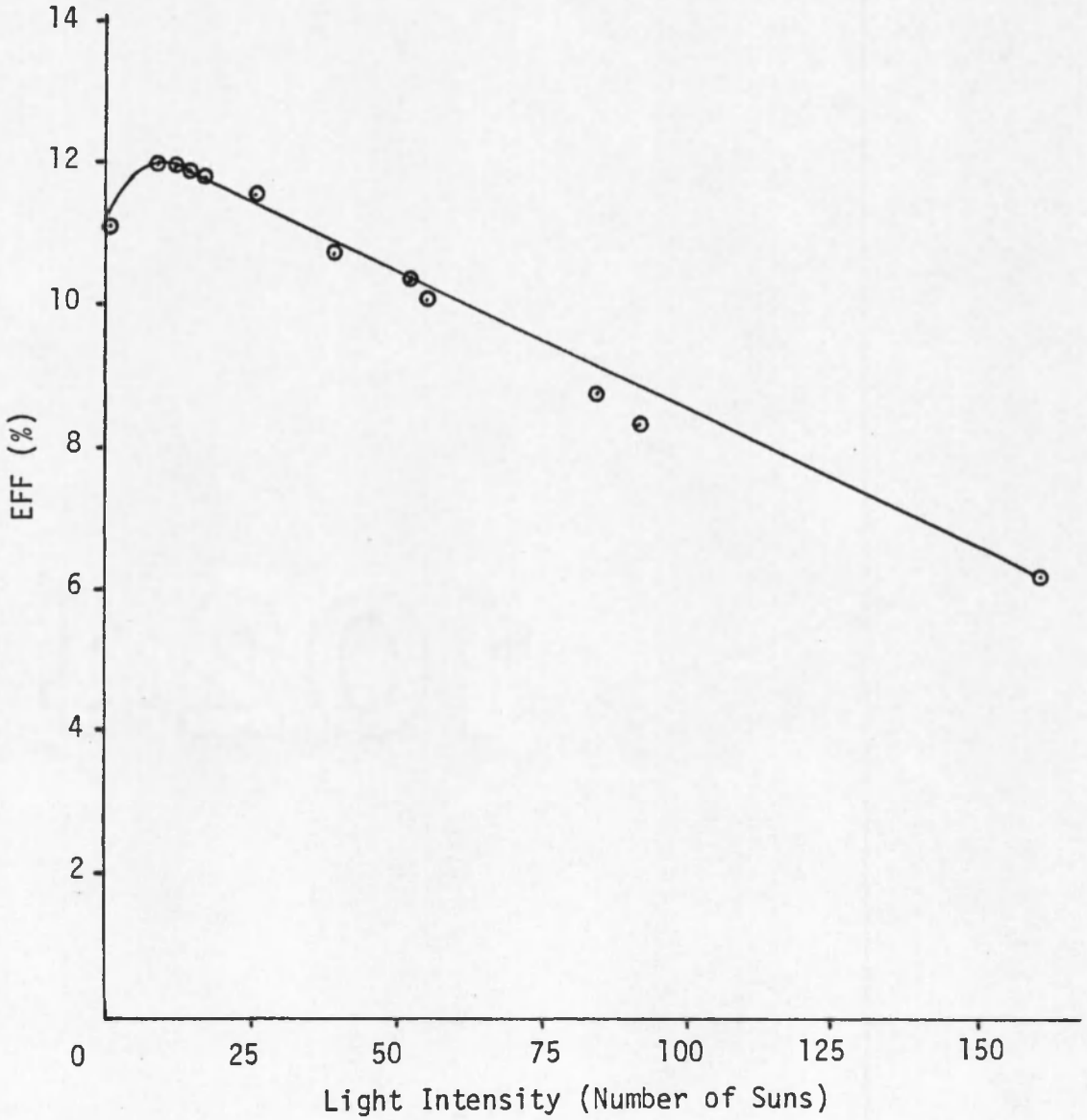

Fig. 10. Continued. Cell 17-12--22.5 Fingers/cm.

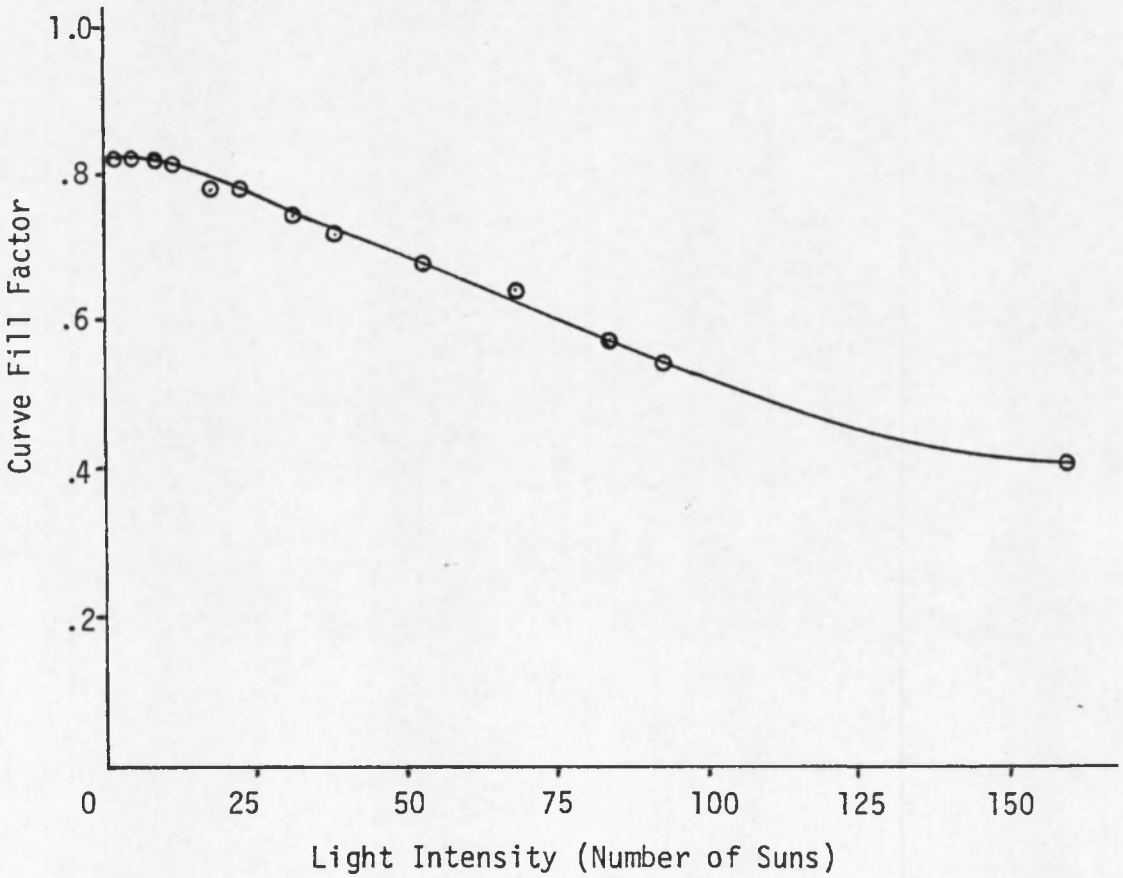

Fig. 10. Continued. Cell 17-12--22.5 Fingers/cm.

Table 18. Pattern B--Cell 15-6, 30 Fingers/cm.

Number of Suns	I_{sc}	V_{oc}	EFF	CFF
8	.7	.60	10.6	.811
15	1.3	.61	10.6	.805
30	2.6	.615	10.0	.760
44	3.8	.615	9.1	.690
93	8.0	.615	7.9	.600
122	10.4	.632	7.0	.520
155	13.3A	.635	6.1	.450

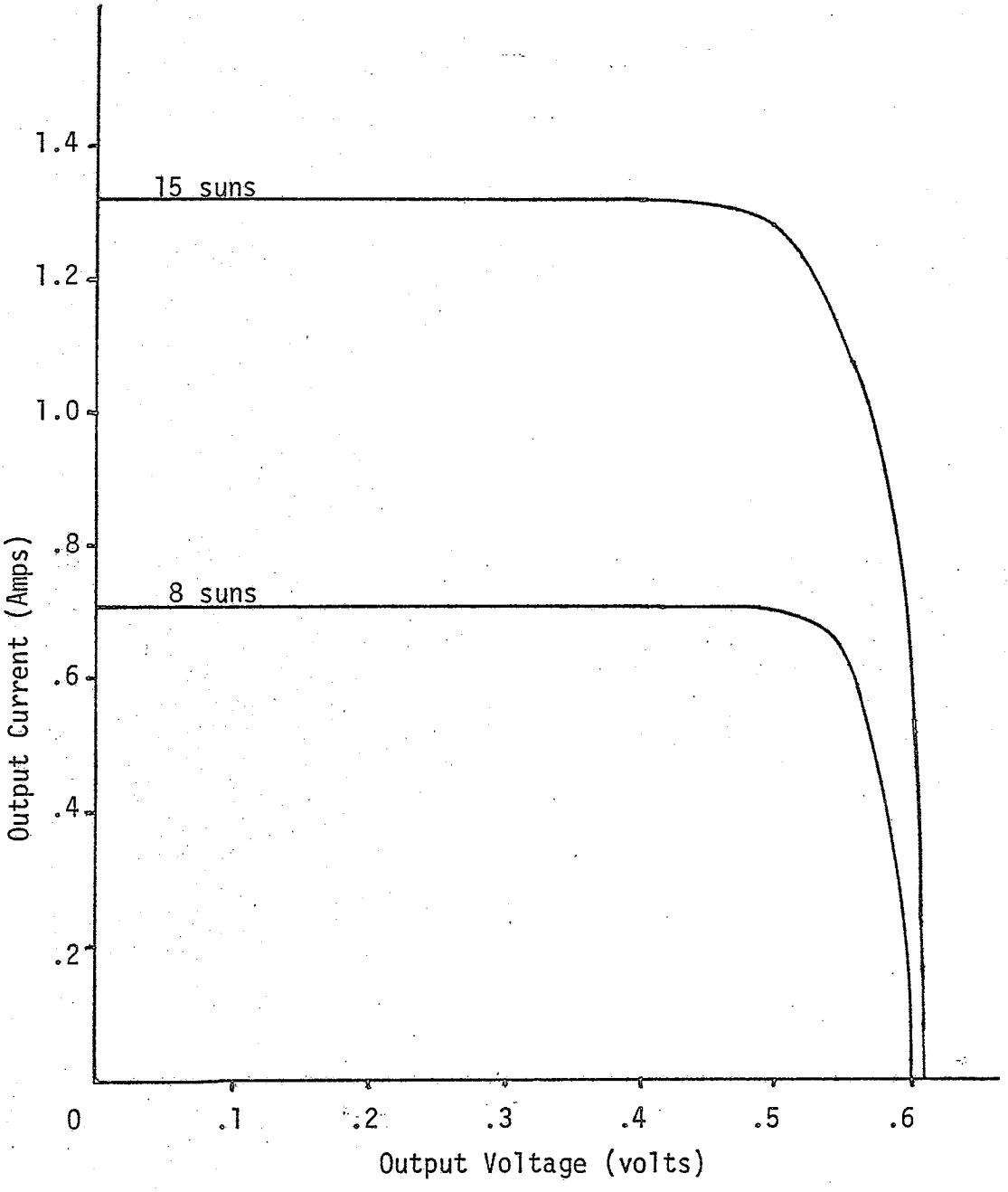

Fig. 11. Cell 15-6--30 Fingers/cm.

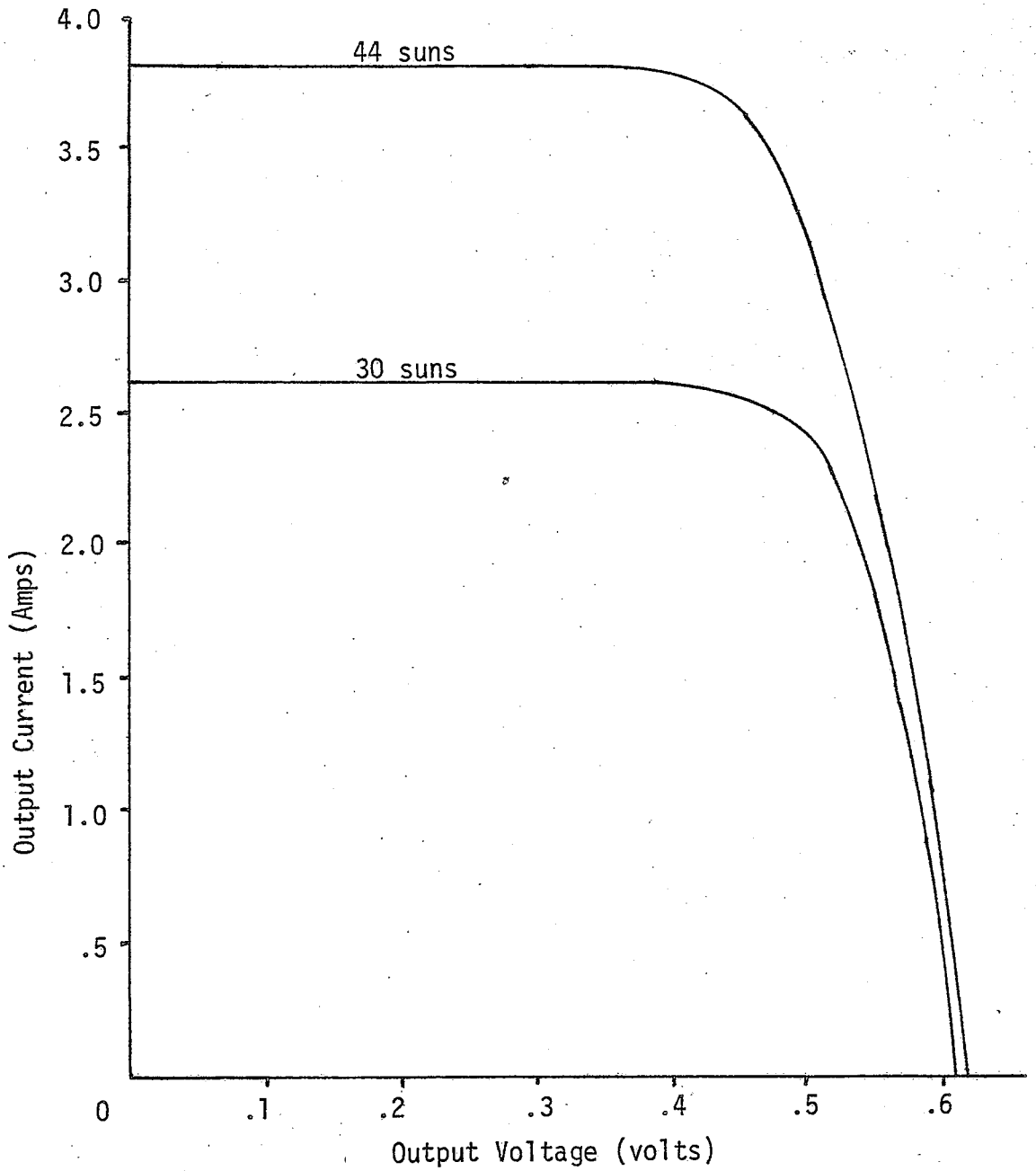

Fig. 11. Continued. Cell 15-6--30 Fingers/cm.

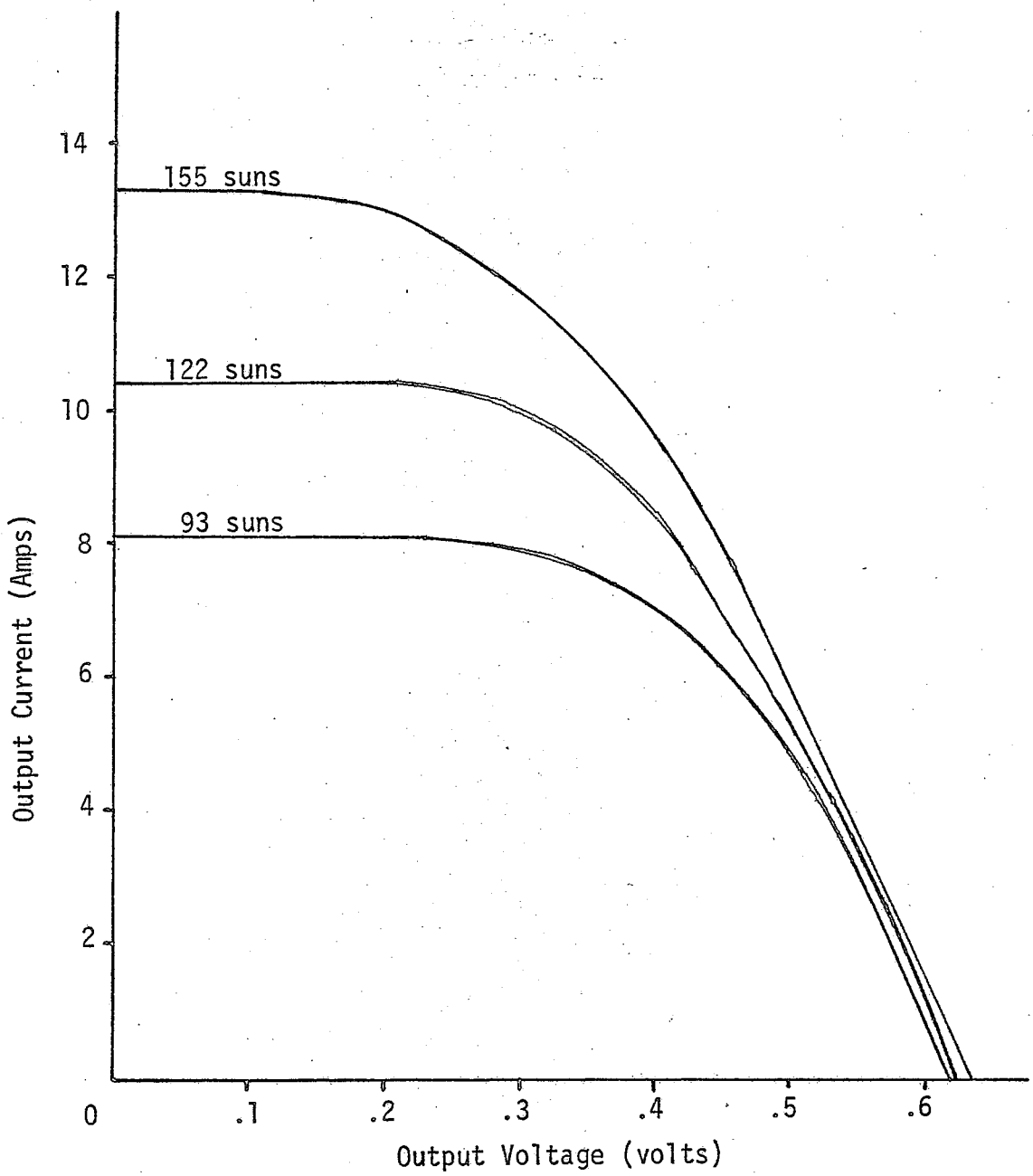

Fig. 11. Continued. Cell 15-6--30 Fingers/cm.

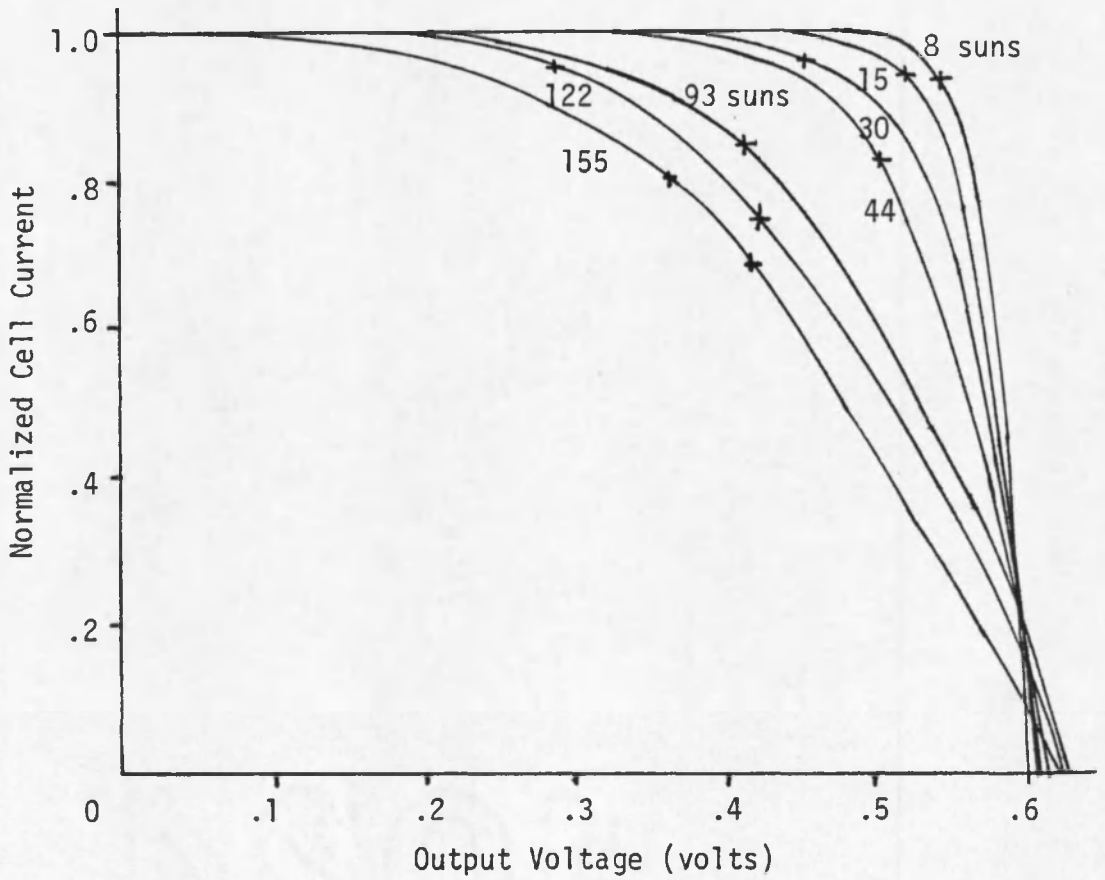

Fig. 11. Continued. Cell 15-6--30 Fingers/cm.

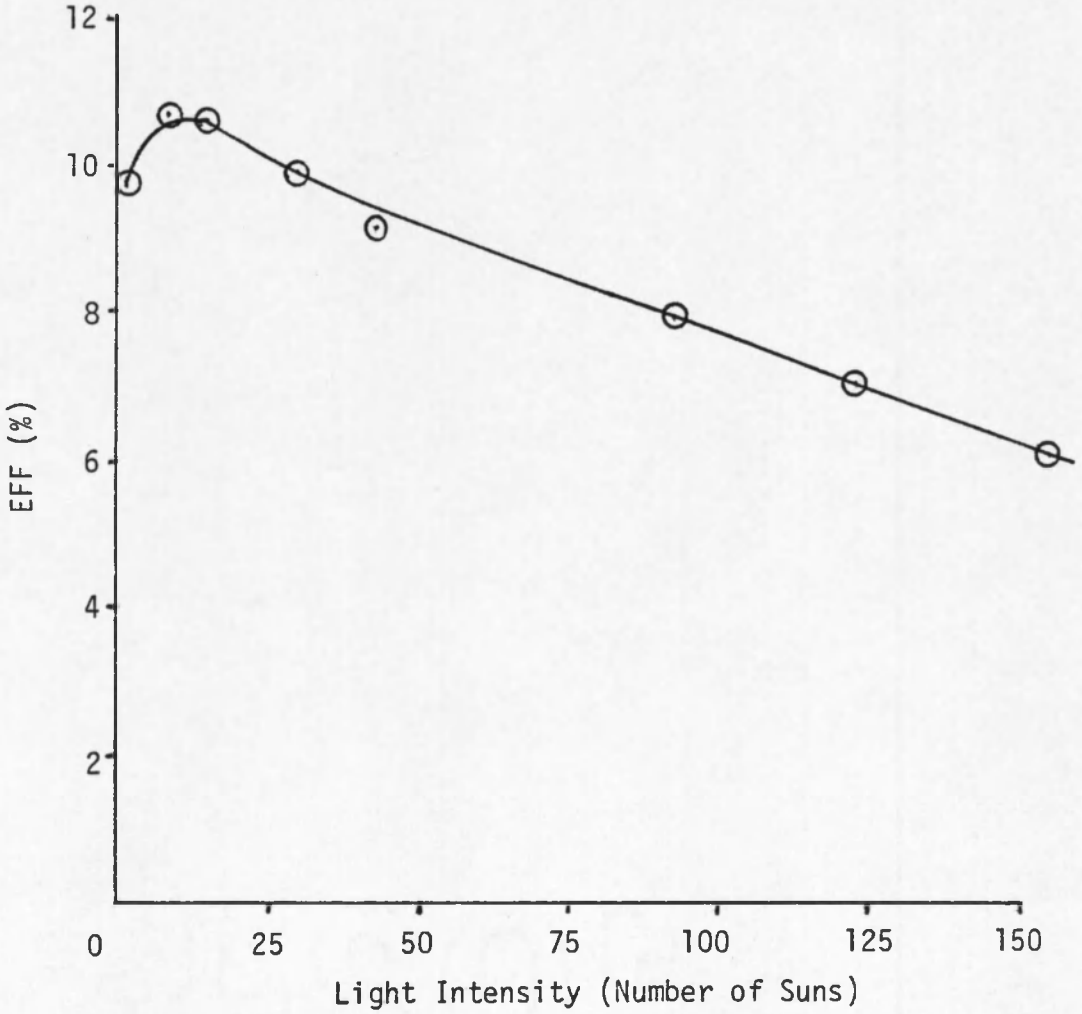

Fig. 11. Continued. Cell 15-6--30 Fingers/cm.

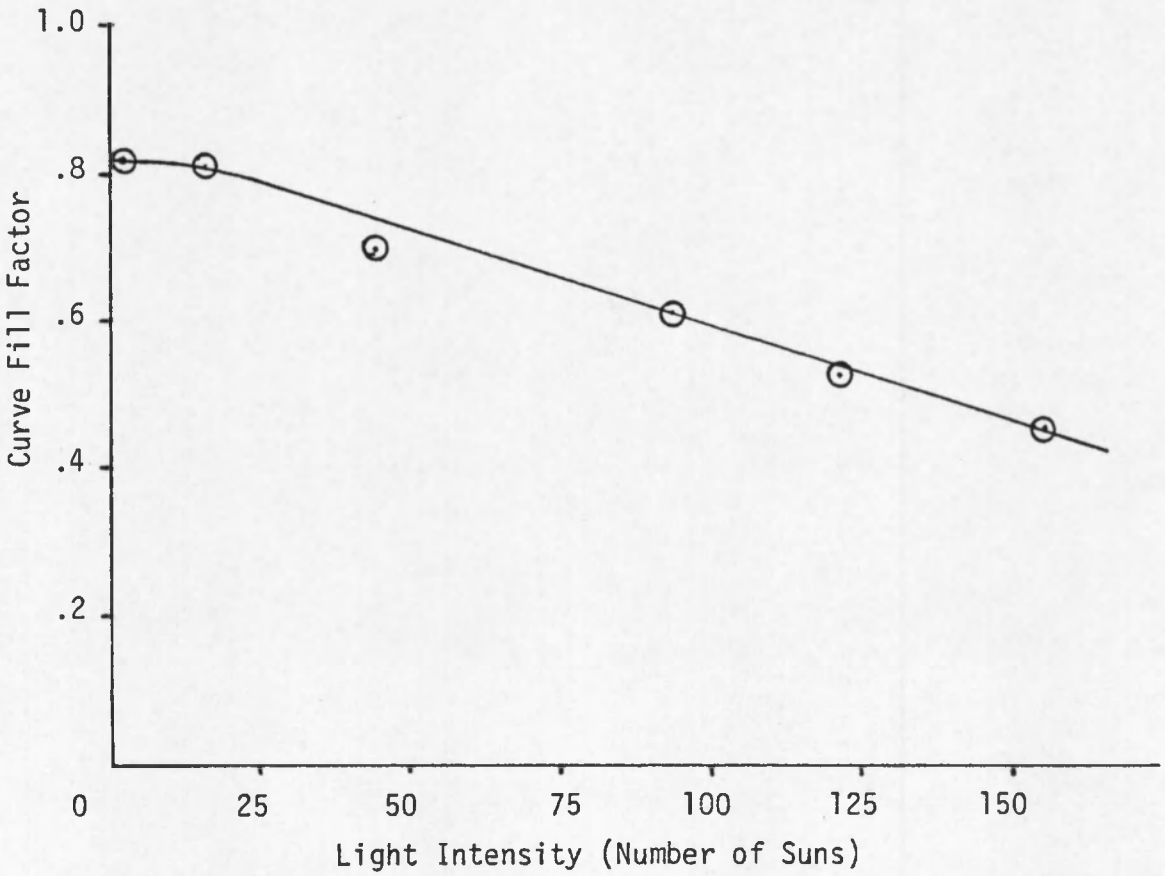

Fig. 11. Continued. Cell 15-6--30 Fingers/cm.

Table 19. Pattern C--Cell 14-15, 30 Fingers/cm with 2 Mains.

Number of Suns	I_{sc}	V_{oc}	EFF	CFF
170	14.5A	.650	7.1	.47
130	11.0	.649	7.3	.54
115	9.8	.645	7.8	.58
70	5.9	.638	8.5	.64
51	4.3	.636	9.2	.68
30	2.6	.632	9.5	.72
17	1.4	.621	10.0	.76

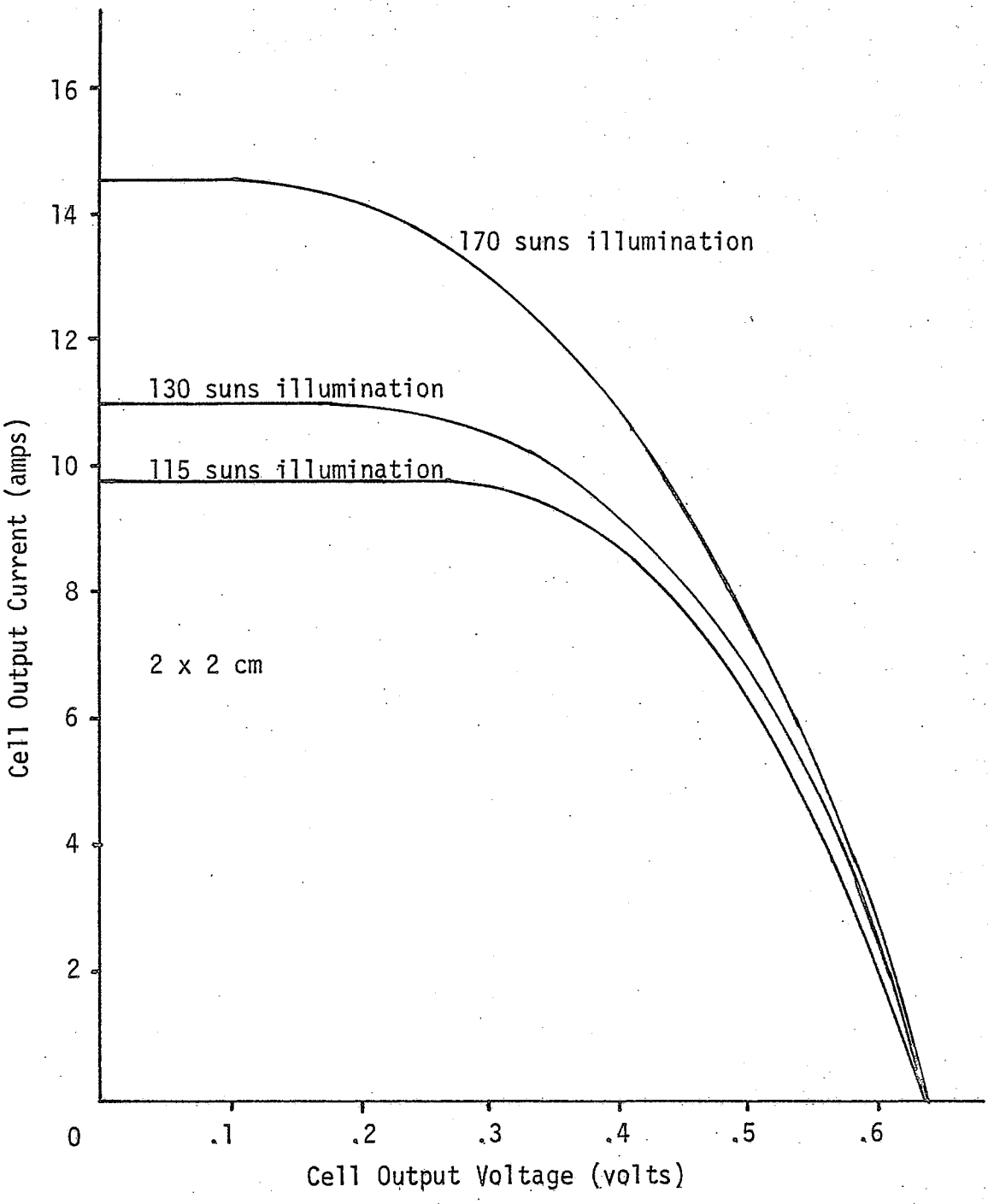

Fig. 12. Cell 14-15--30 Fingers/cm with 2 Mains, V-I Curve for Cell Illuminated with 170 Suns.

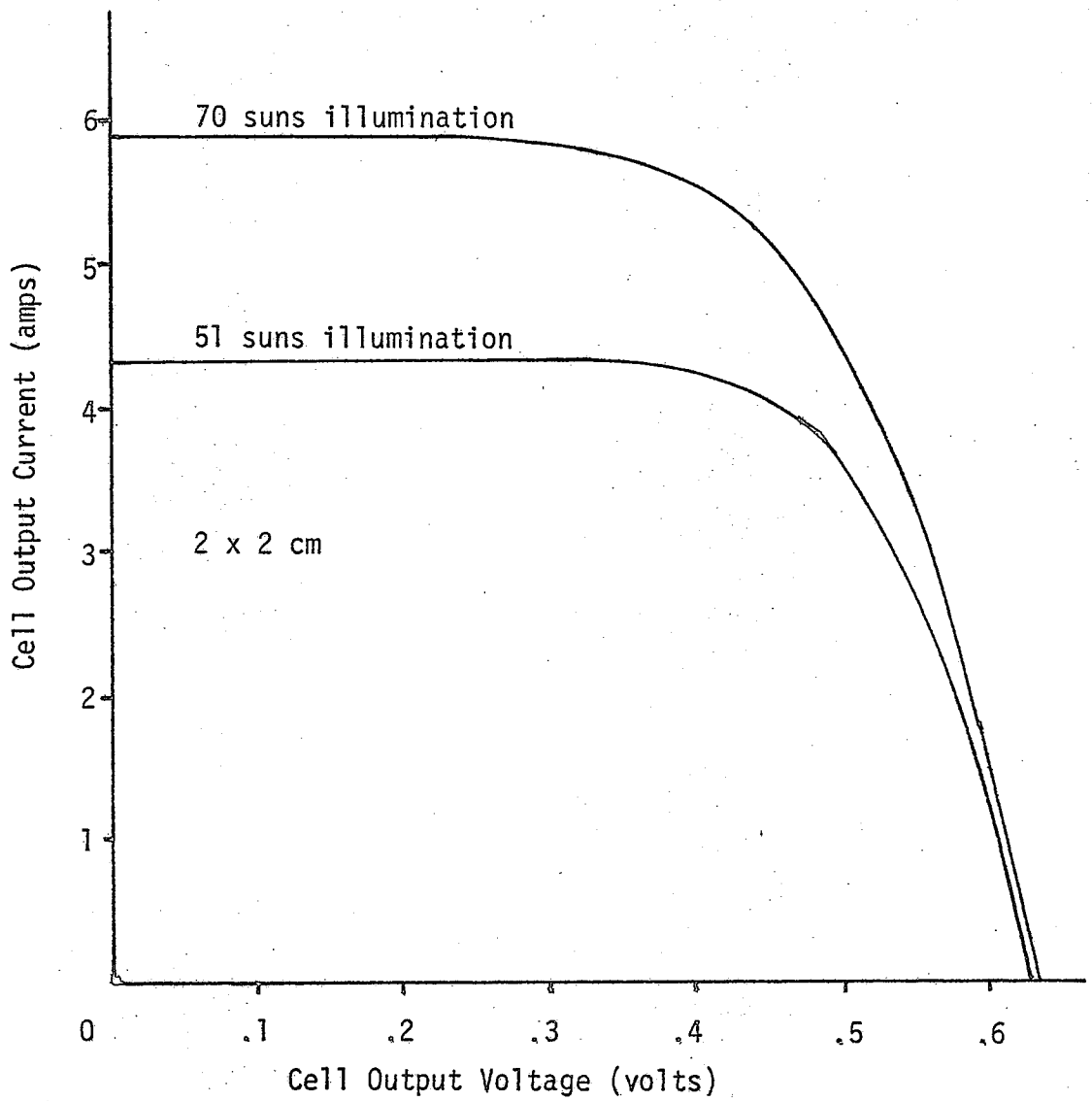

Fig. 13. Cell 14-15--30 Fingers/cm with 2 Mains, V-I Curve for Cell Illuminated with 70 Suns.

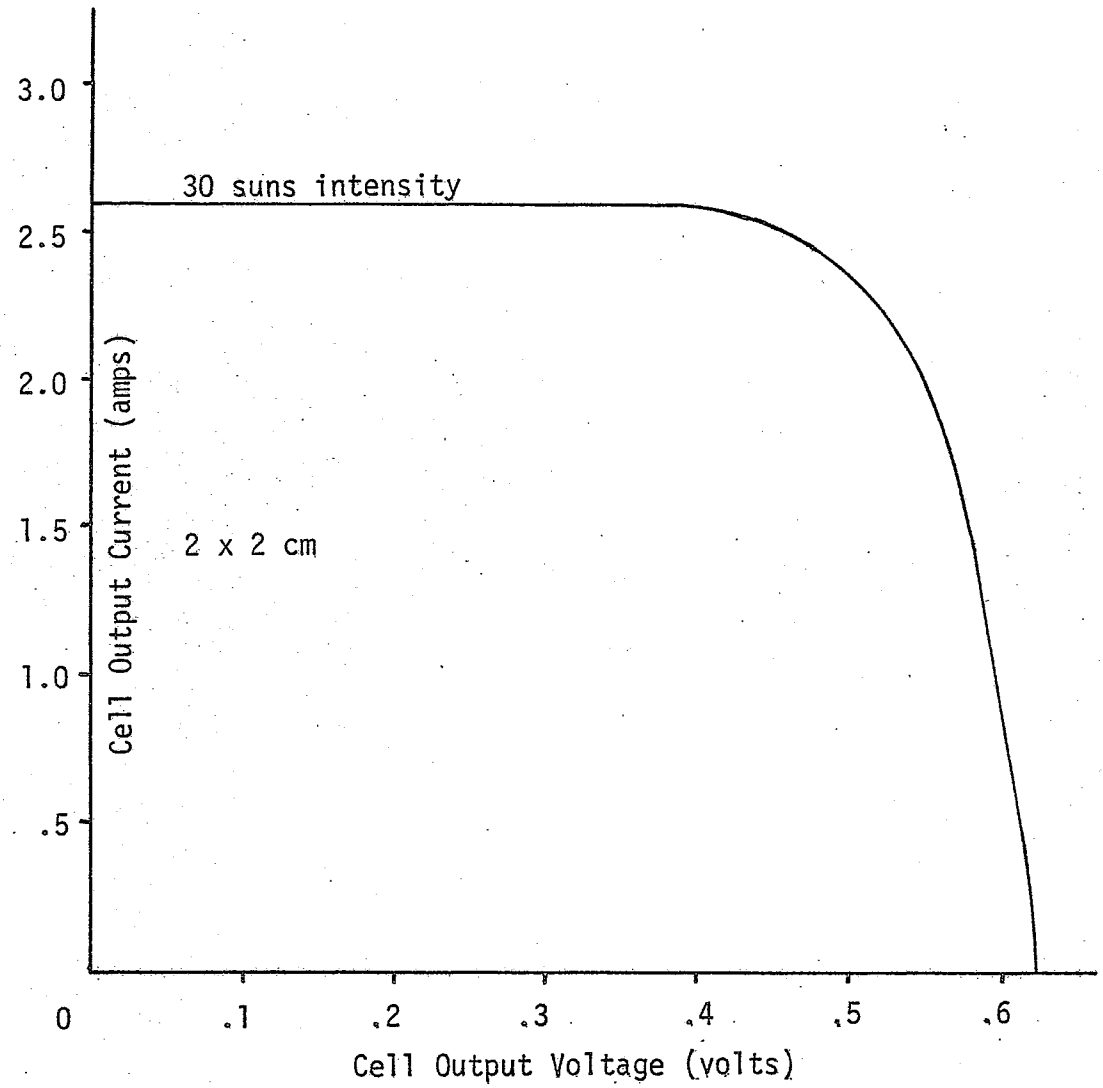

Fig. 14. Cell 14-15--30 Fingers/cm with 2 Mains, V-I Curve for Cell Illuminated with 30 Suns.

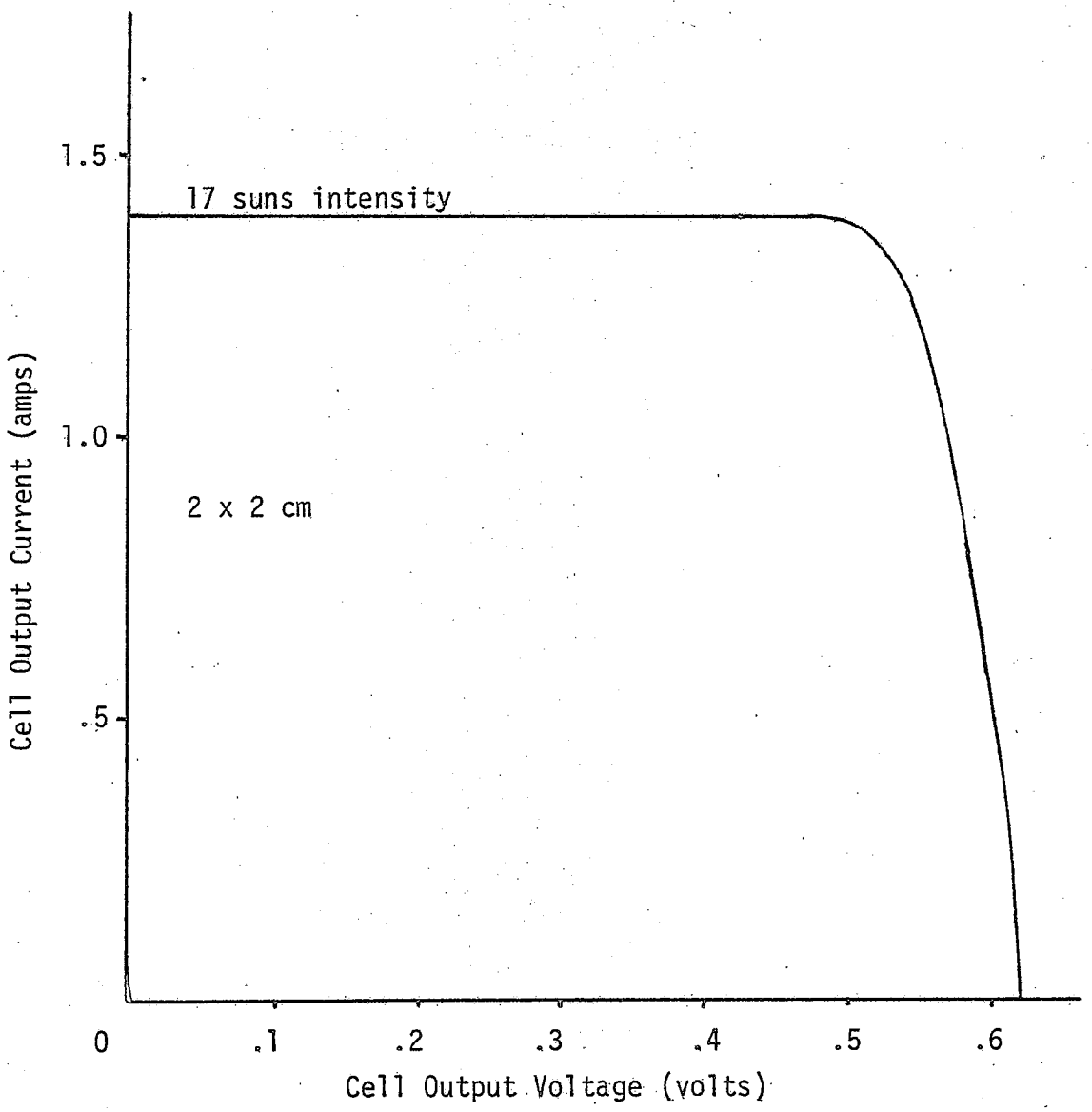

Fig. 15. Cell 14-15--30 Fingers/cm with 2 Mains, V-I Curve for Cell Illuminated with 17 Suns.

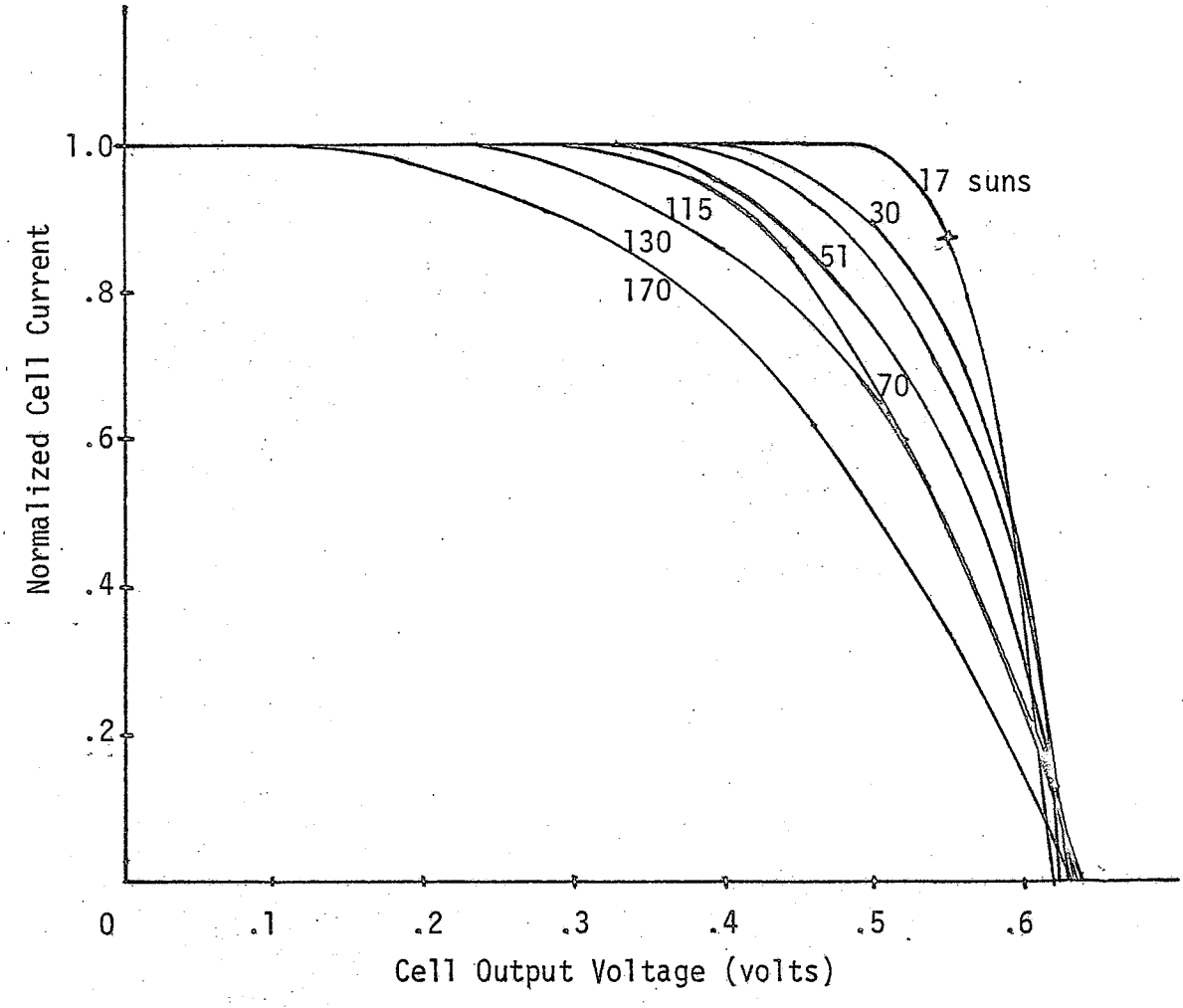

Fig. 16. Cell 14-15--30 Fingers/cm with 2 Mains, Normalized Comparison of Cell Exposed to Different Sun Intensities.

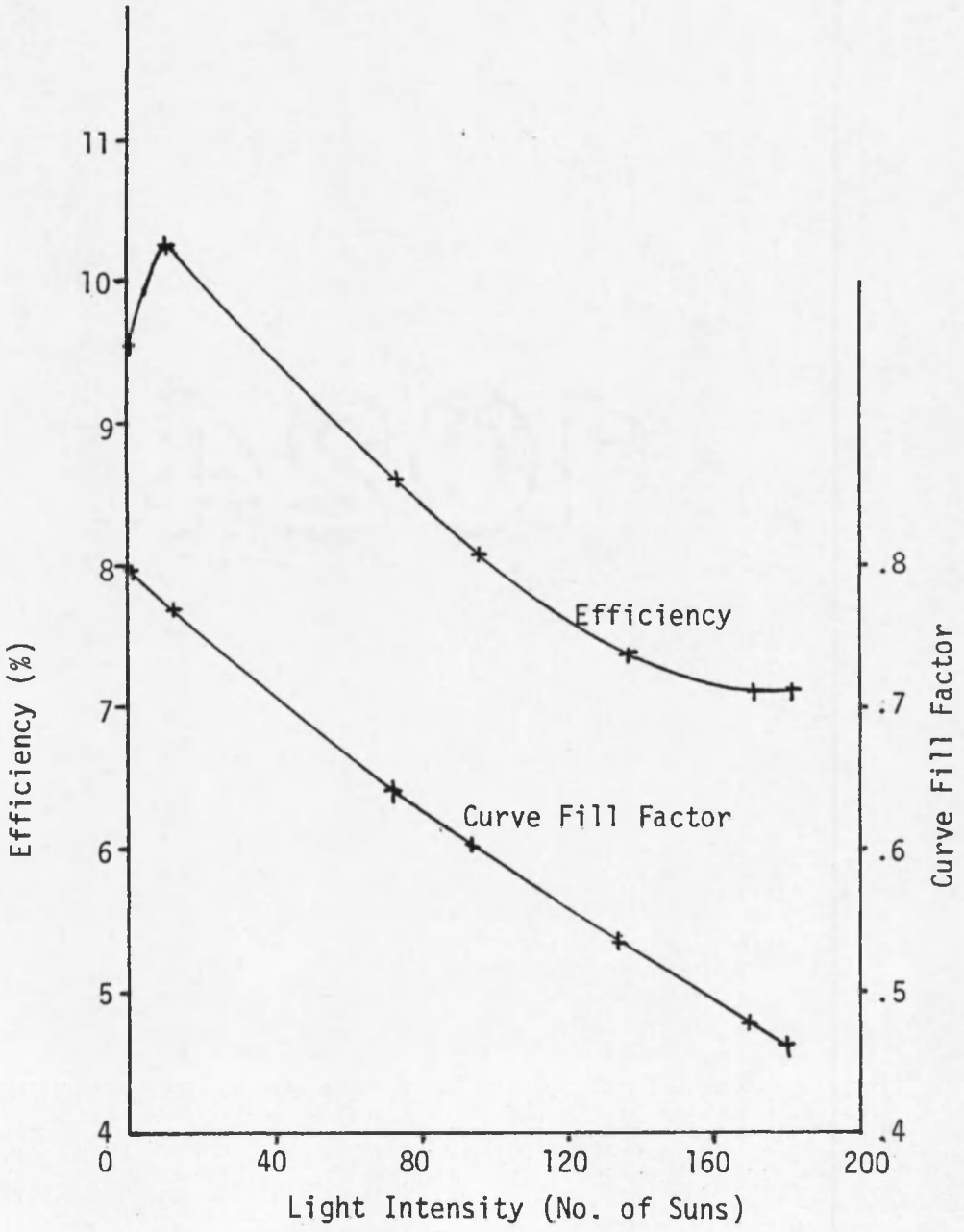

Fig. 17. Cell 14-15--30 Fingers/cm with 2 Mains, Efficiency and Curve Fill Factor versus Light Intensity.

Table 20. Pattern D--Cell 14-11, 15 Fingers/cm.

Number of Suns	I_{sc}	V_{oc}	EFF	CFF
104.0	9.70	.58	6.2	.46
86.0	8.00	.60	6.8	.49
67.0	6.30	.60	7.6	.55
56.0	5.20	.60	8.1	.58
37.0	3.40	.60	8.8	.64
30.0	2.80	.60	9.2	.67
1.4	.13	.57	10.5	.79

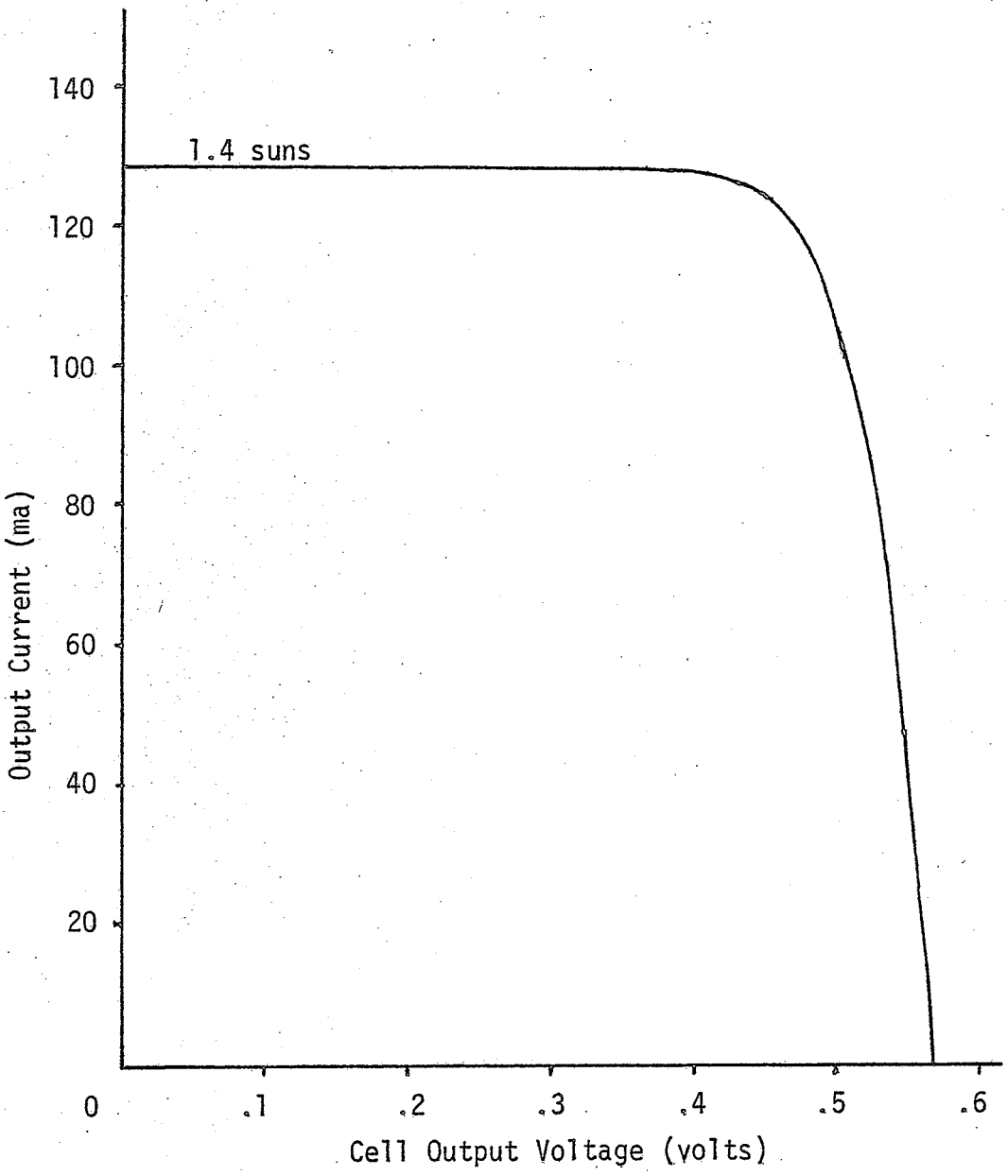

Fig. 18. Cell 14-11--15 Fingers/cm.

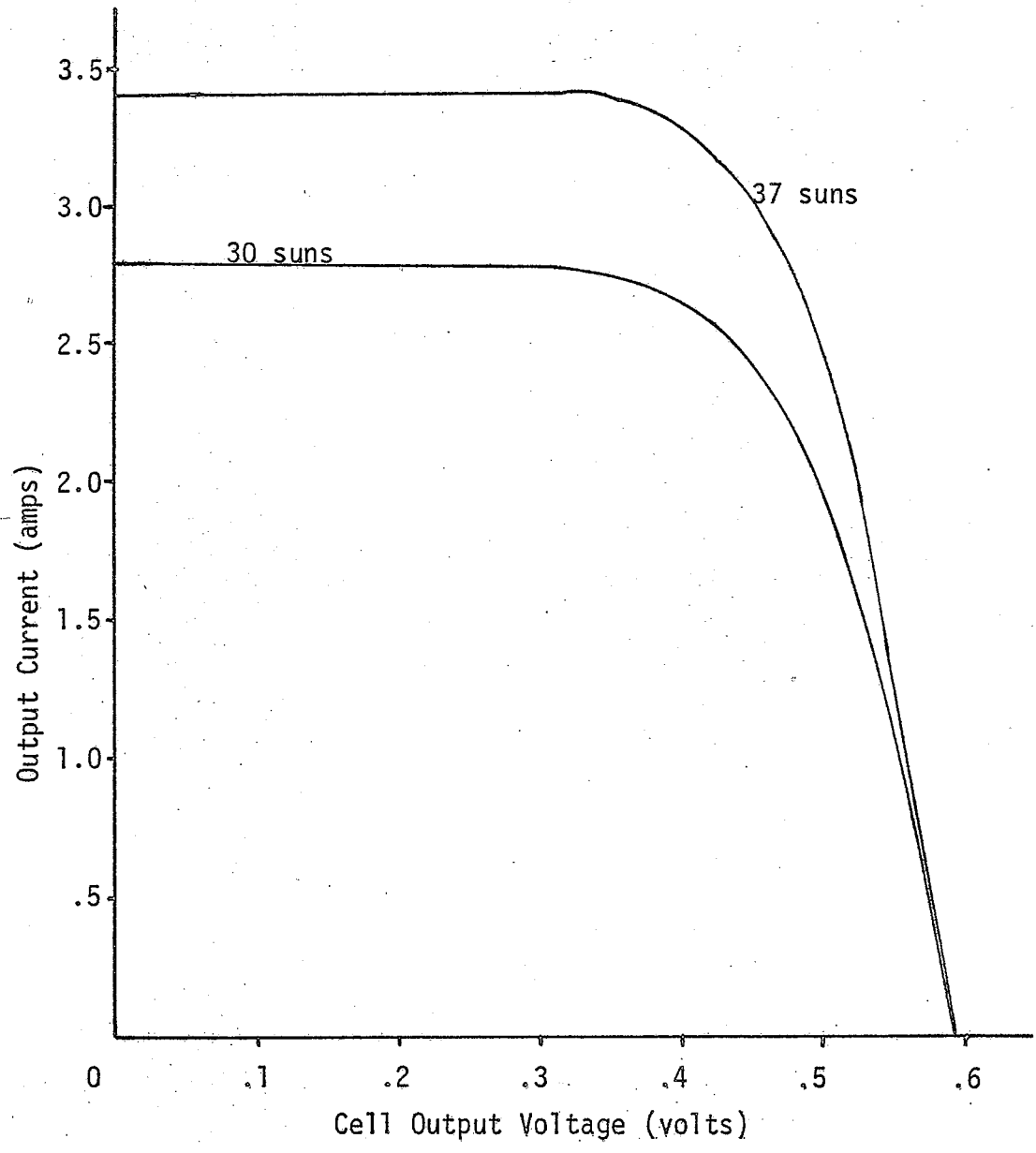

Fig. 18. Continued. Cell 14-11--15 Fingers/cm.

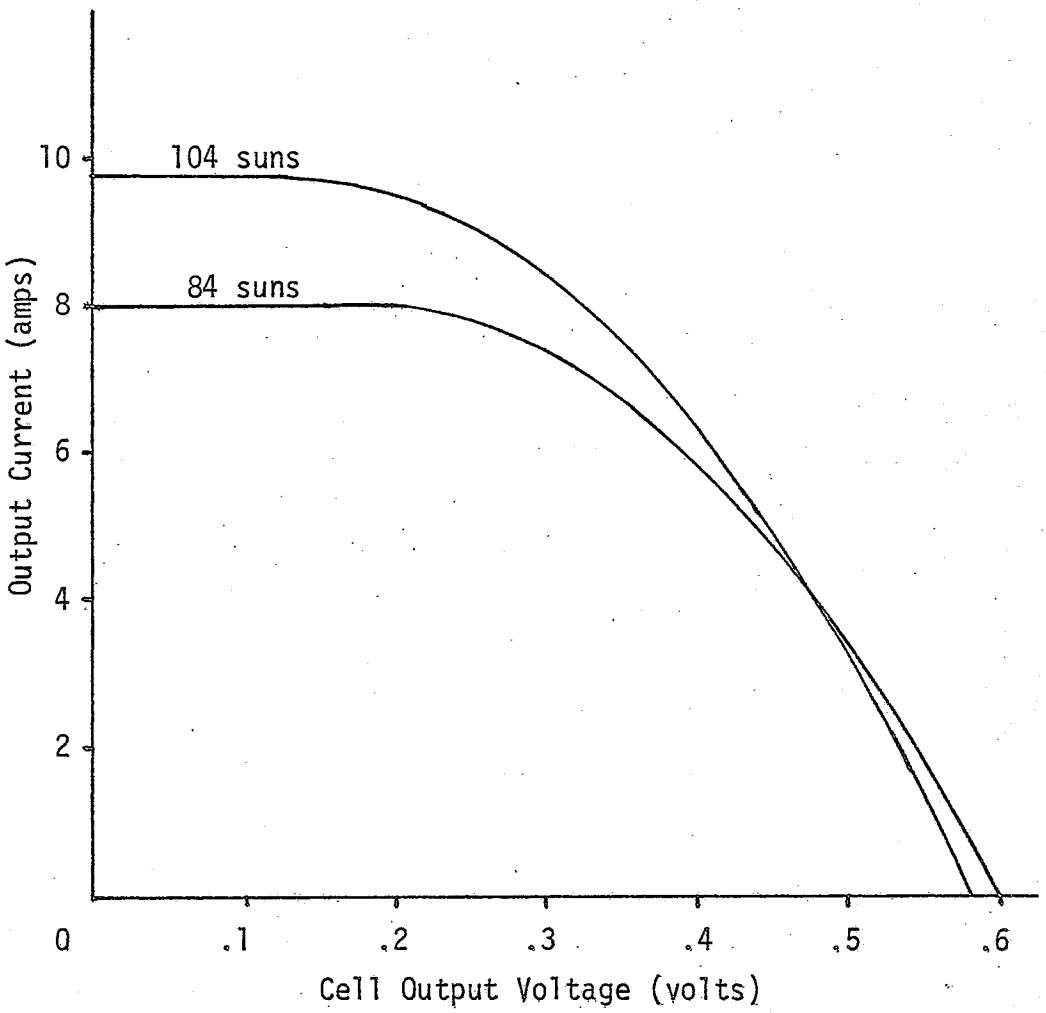

Fig. 18. Continued. Cell 14-11--15 Fingers/cm.

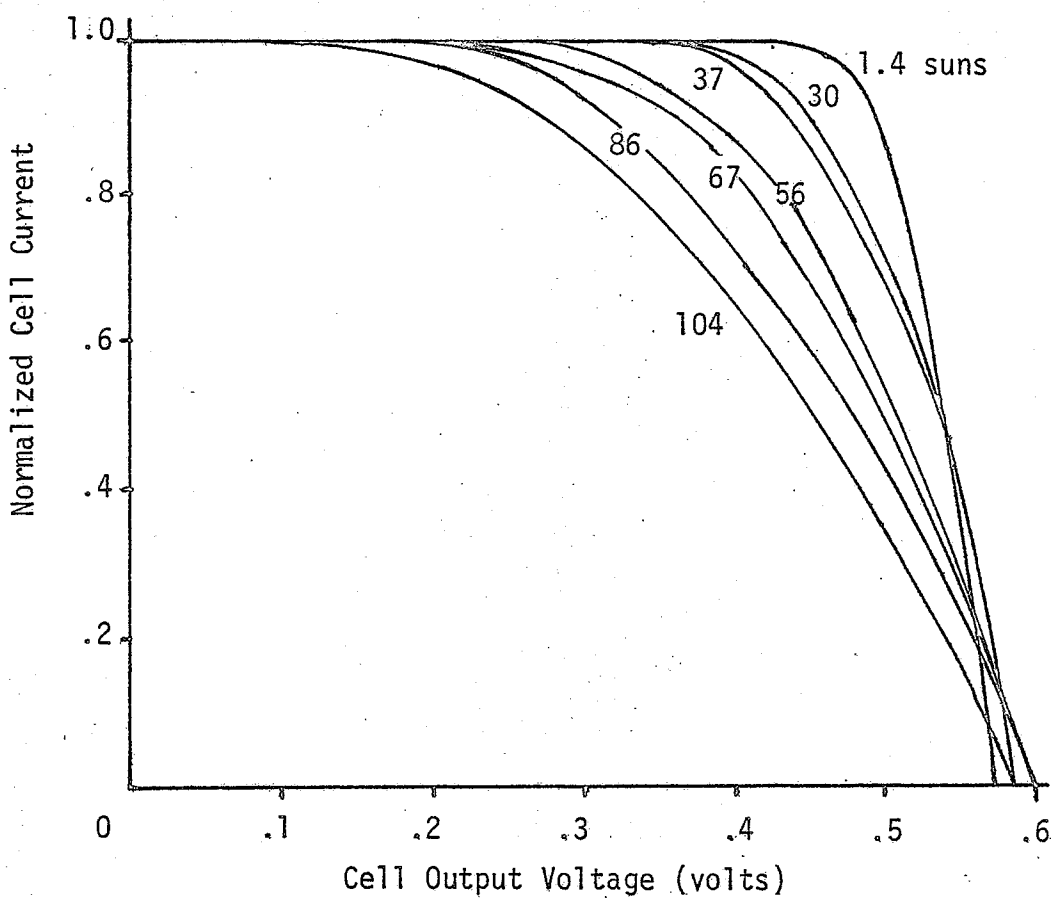

Fig. 18. Continued. Cell 14-11--15 Fingers/cm.

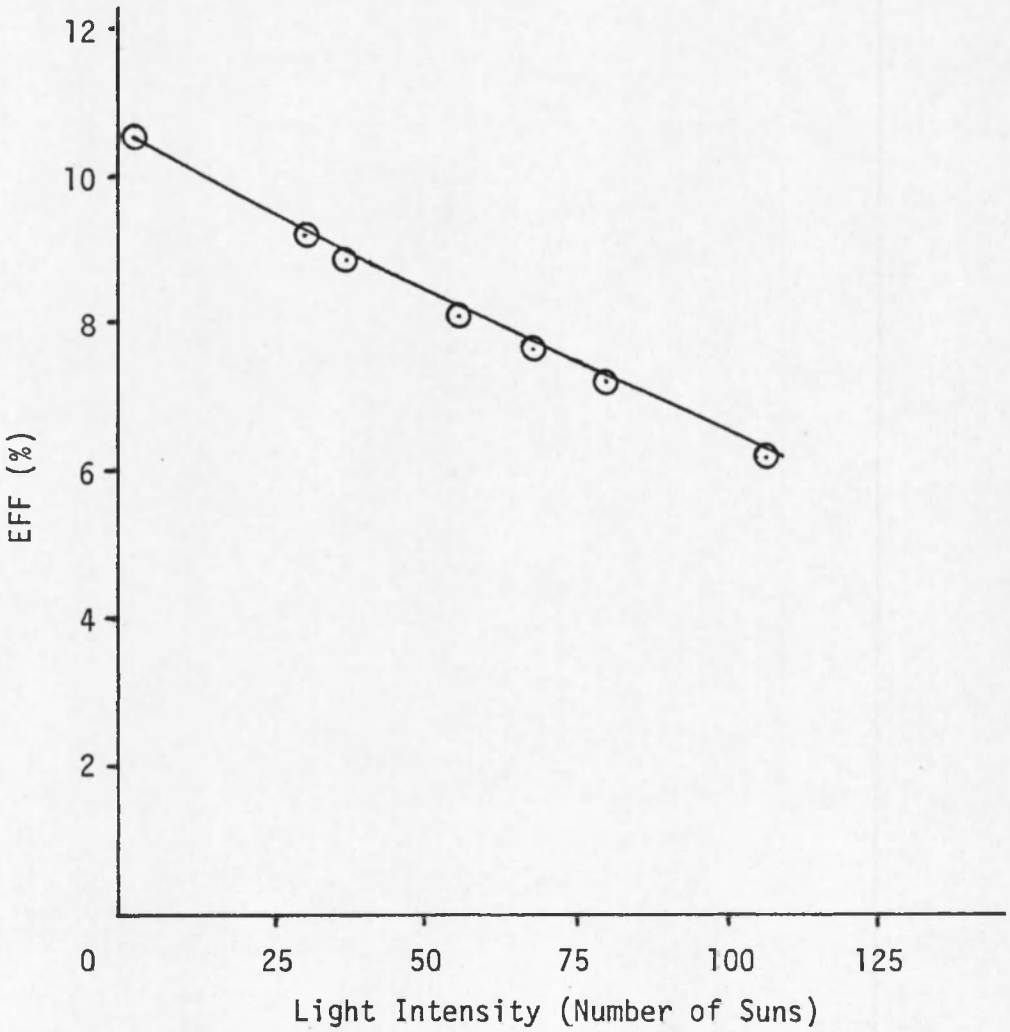

Fig. 18. Continued. Cell 14-11--15 Fingers/cm.

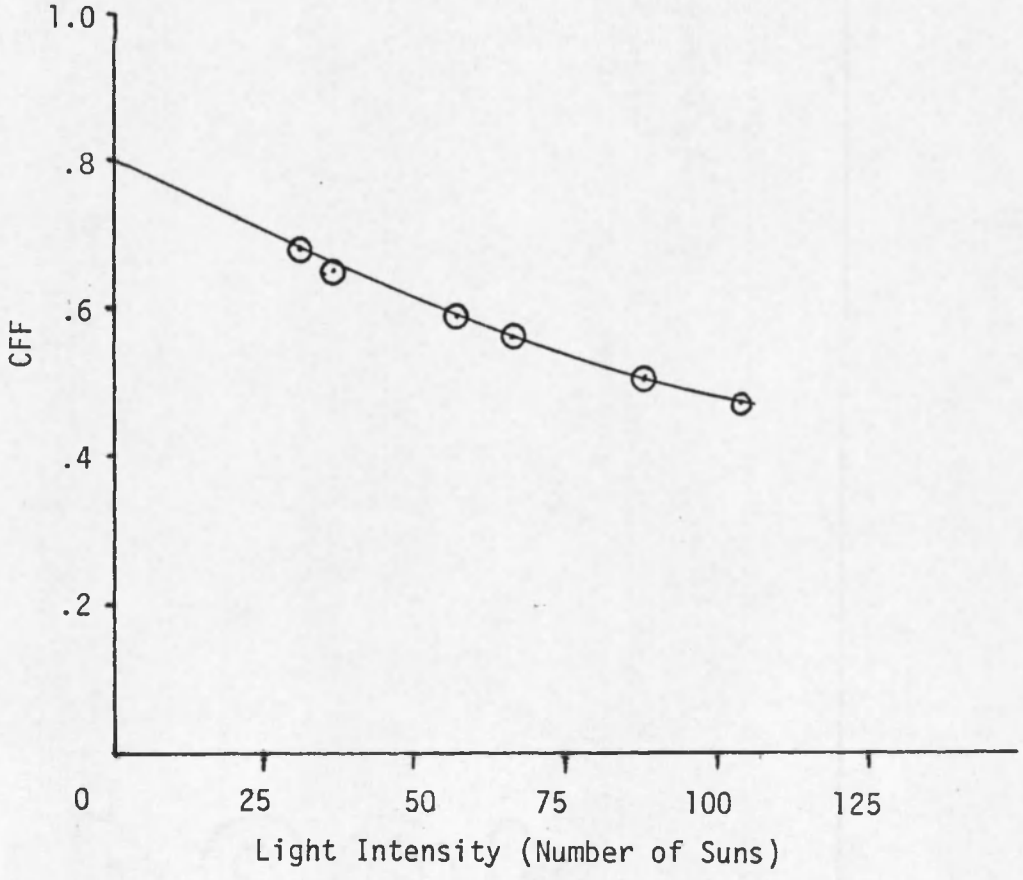

Fig. 18. Continued. Cell 14-11--15 Fingers/cm.

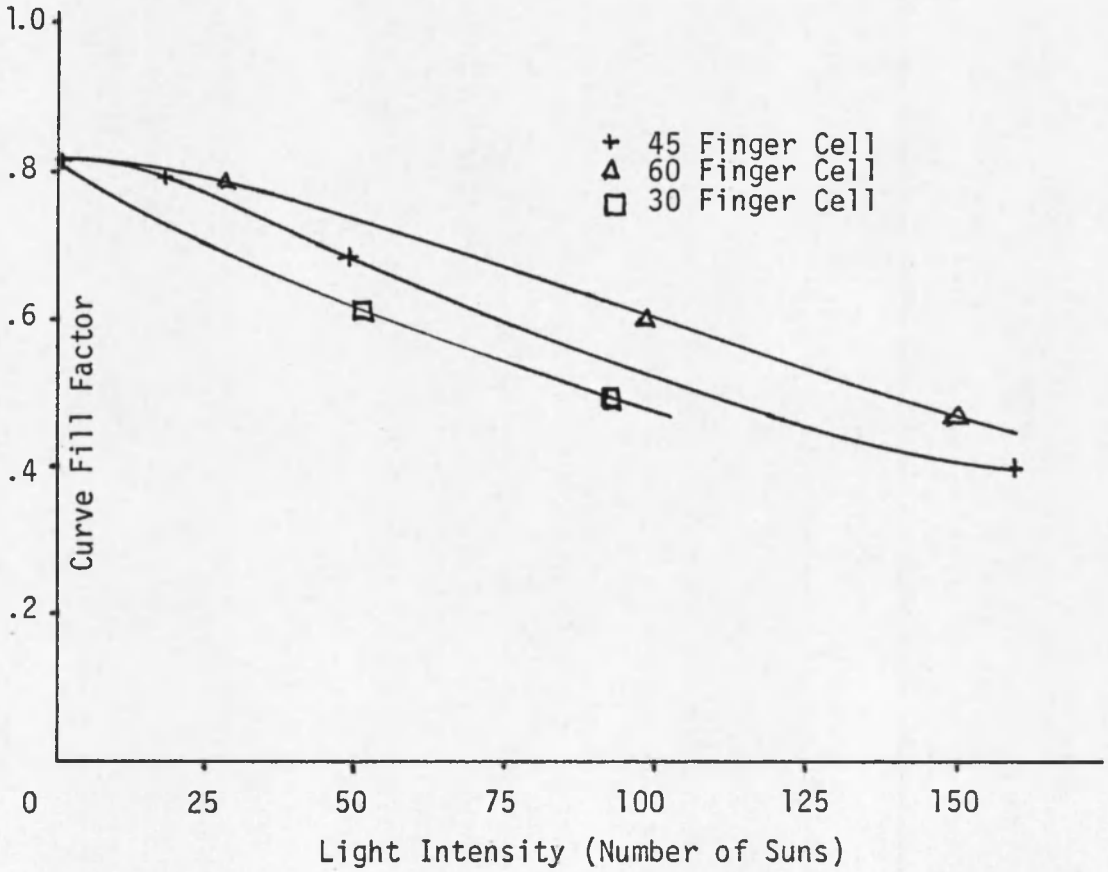

Fig. 18. Continued. Cell 14-11--15 Fingers/cm.

Table 21. Pattern E--Cell 14-3, 15 Fingers/cm with 3 Mains.

Number of Suns	I_{sc}	V_{oc}	EFF	CFF
1	0.093A	.575	10.5	.788
23	2.15	.634	10.3	.6984
28	2.6	.634	10.54	.7146
37	3.42	.64	10.6	.7127
52	4.8	.646	10.38	.640
72	6.65	.647	9.60	.638
84	7.8	.648	9.07	.601
91	8.5	.640	8.93	.6
176	16.35A	.625	5.80	.399
216	20.0	.615	5.8	.405

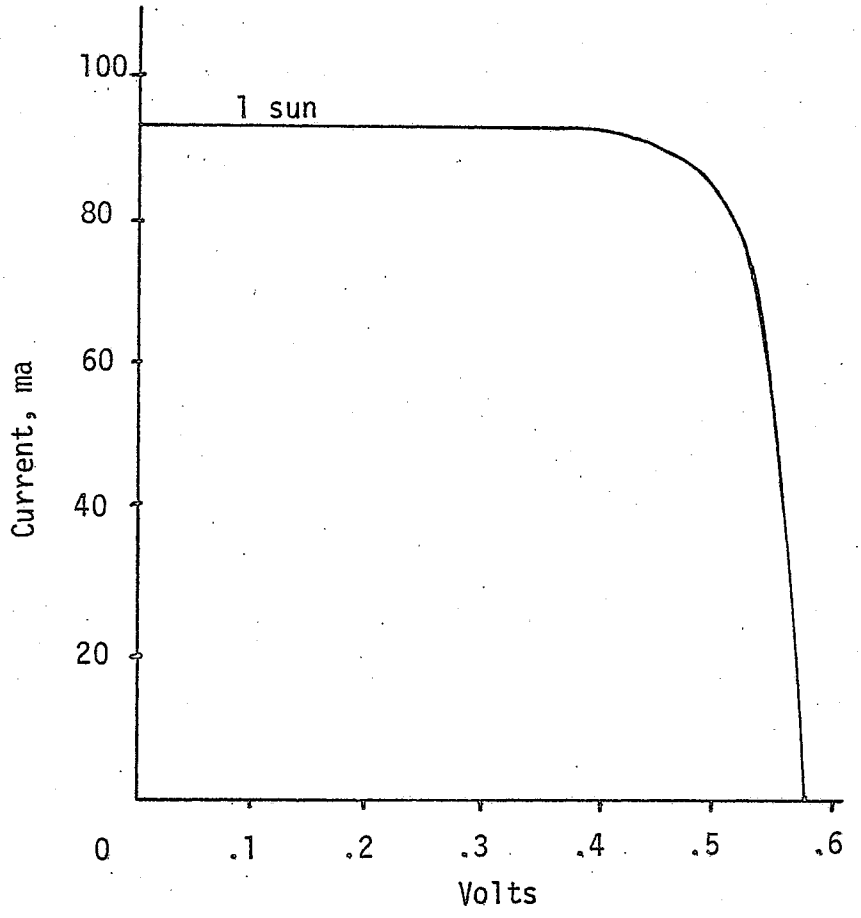

Fig. 19. Cell 14-3--15 Fingers/cm with 3 Mains.

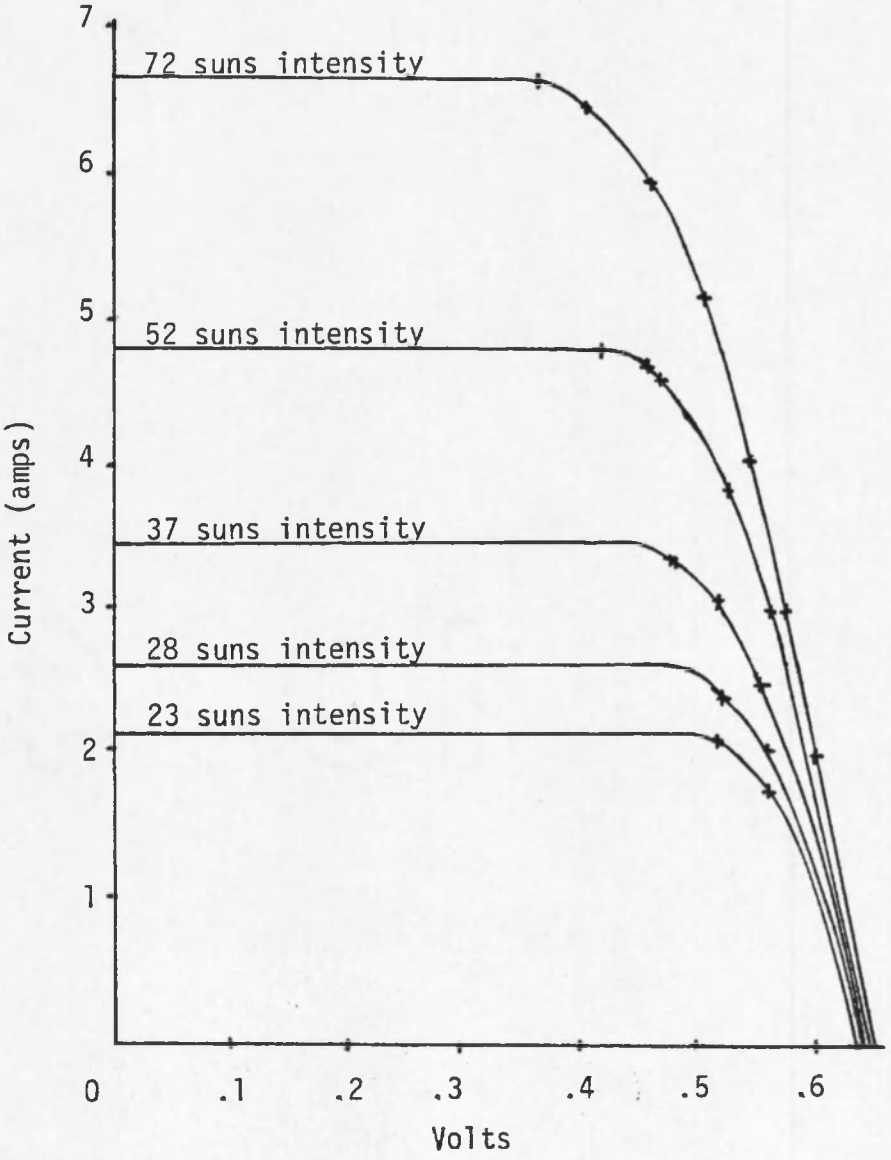

Fig. 19. Continued. Cell 14-3--15 Fingers/cm with 3 Mains.

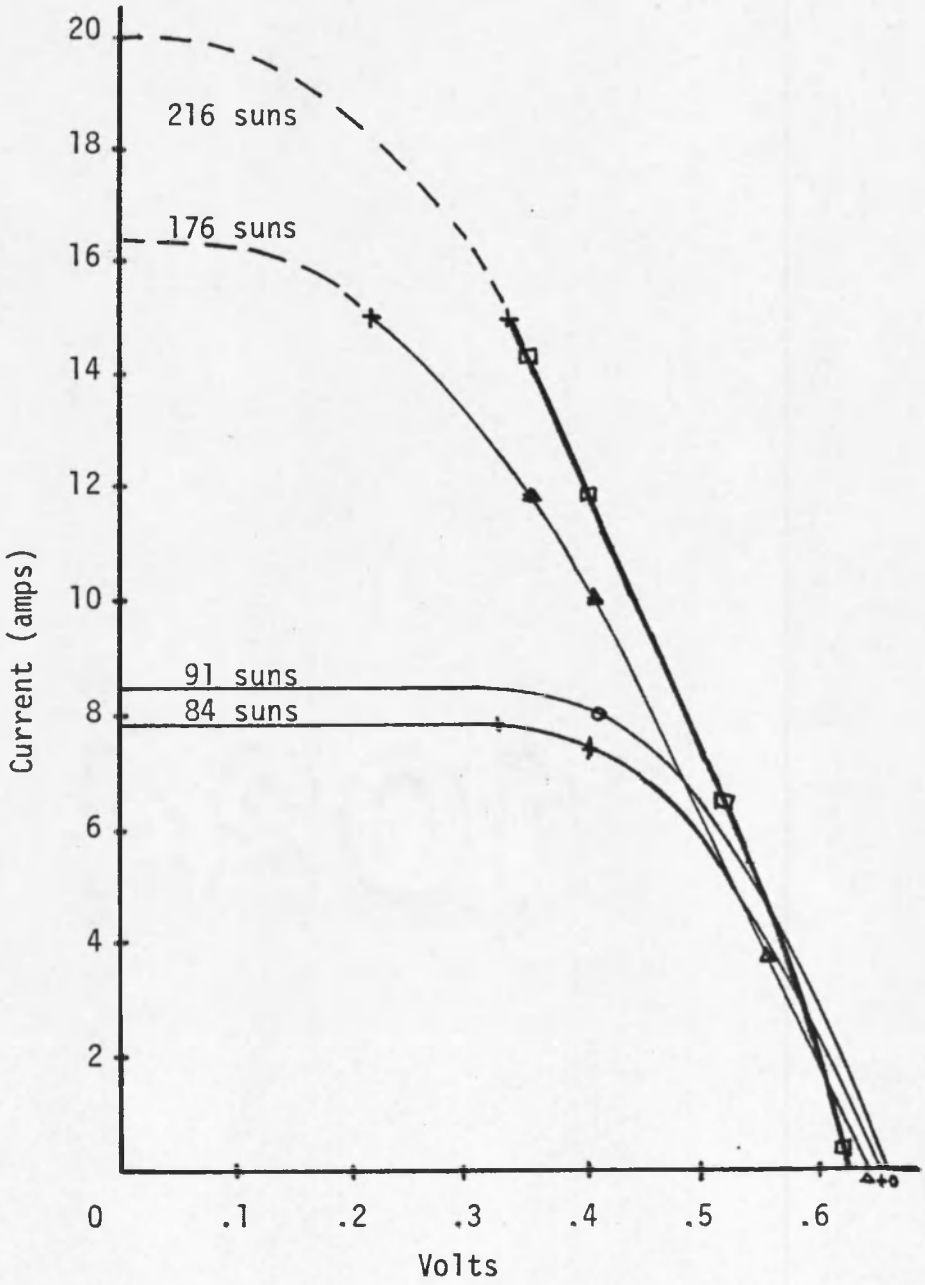

Fig. 19. Continued. Cell 14-3--15 Fingers/cm with 3 Mains.

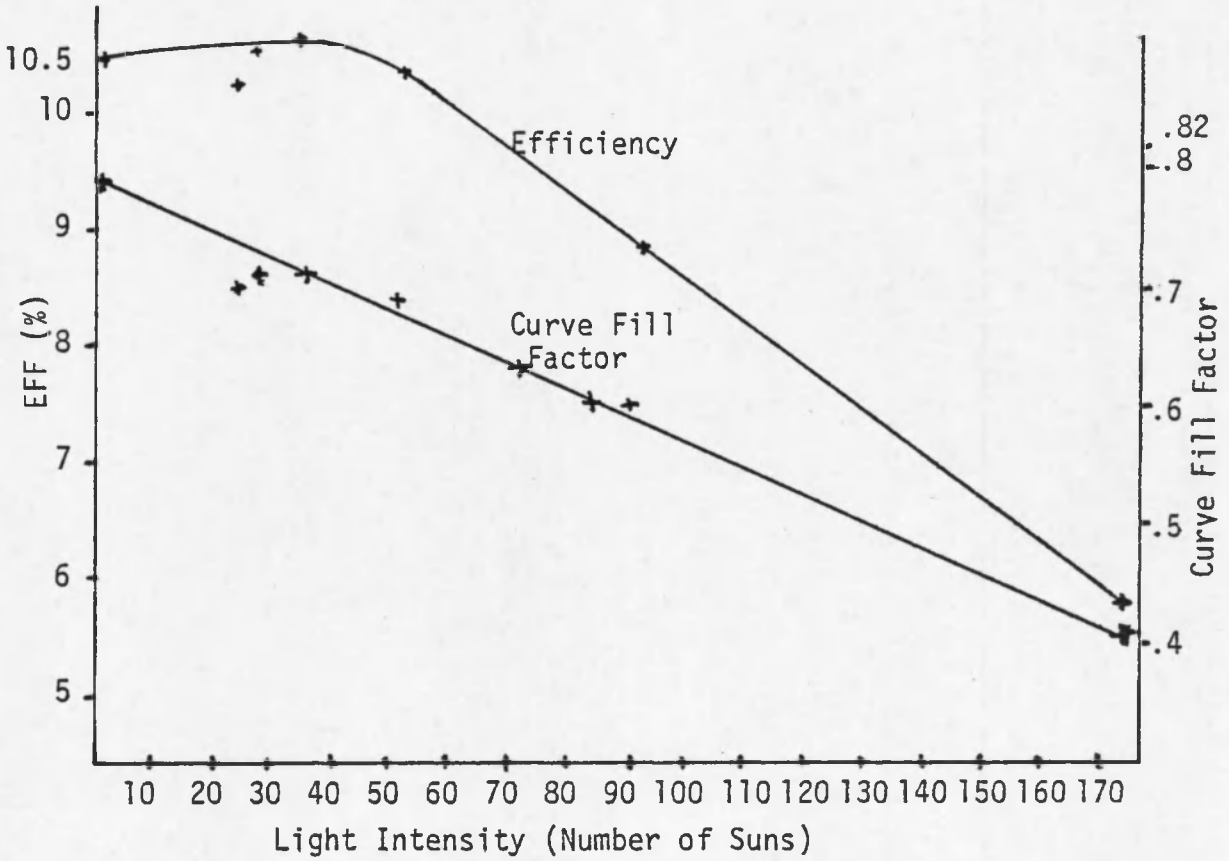

Fig. 19. Continued. Cell 14-3--15 Fingers/cm with 3 Mains.

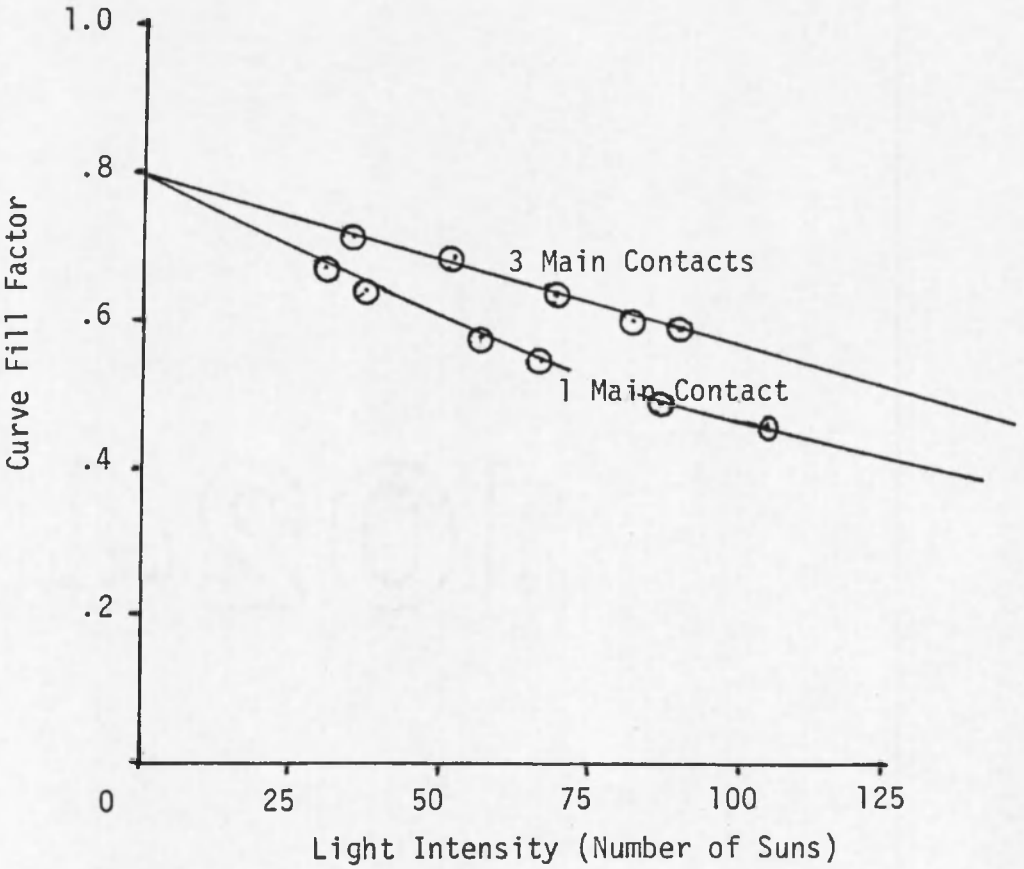

Fig. 20. Cell 14-3--15 Fingers/cm with 3 Mains, Comparison of CFF for 30 Finger Cell with 1 Main Contact and 3 Main Contacts.

Table 22. Pattern F--Clover-leaf Pattern.

Number of Suns	I_{sc}	V_{oc}	EFF	CFF
1.4	0.6A	2.0	10.12	0.75
3.15	1.35	2.54	10.94	0.66
7	3.0	2.5	10.6	0.653
10.97	4.7	2.5	10.3	0.632
13.3	5.7	2.5	9.8	0.600
14.7	6.3	2.42	8.9	0.566

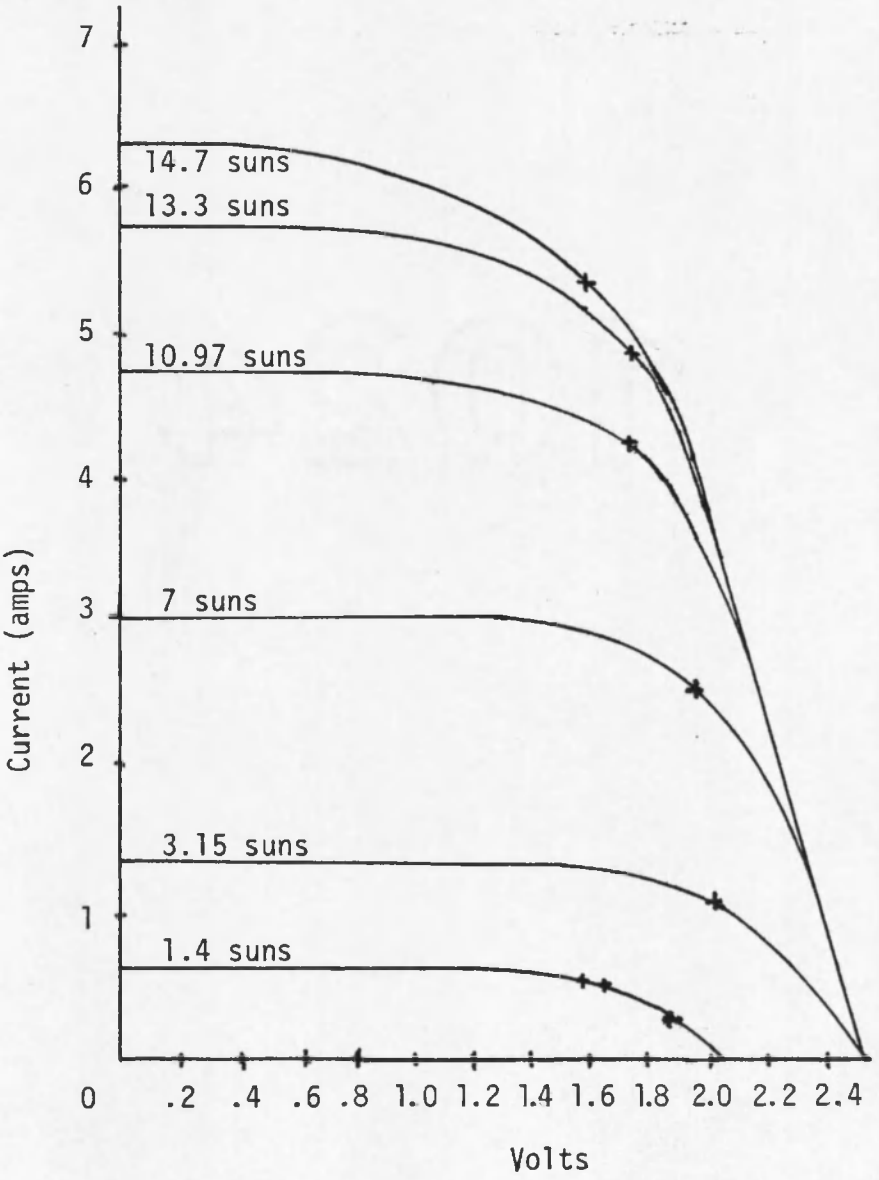

Fig. 21. Clover-leaf Pattern--4 Cells Wired in Series 10 Fingers/cm with 2 Mains.

LIST OF REFERENCES

Angrist, S. W., Direct Energy Conversion, Boston: Allyn and Bacon, Inc., 1971.

Backus, Charles E., Ed., Solar Cells, New York: The Institute of Electrical and Electronics Engineers, Inc., 1976.

Call, R., and W. J. Kerwin, "Concentration Solar Cell," 12th Photovoltaic Specialists Conference, Baton Rough, November 15-18, 1976.

Call, R., and W. J. Kerwin, "Optimization of Solar Cells for High Intensity Illumination," NASA-AMES Research Center, Moffett Field, California, Contract #NCA2-OR040-502, 1976.

Faith, T. J., and A. F. Obenschain, "Temperature, Illumination, and Fluence Dependence of Current and Voltage in Electron Irradiated Solar Cells," NAS-5-21642, U. S. Government Printing Office, Washington, D. C.

Gereth, R., H. Fisher, E. Link, S. Mattes, and W. Pschunder, "Contribution to Silicon Solar Cell Technology," Energy Conversion, Vol. 12, September 1972.

Hamilton, Douglas J., and William G. Howard, Basic Integrated Circuit Engineering, New York, McGraw-Hill, Inc., 1975.

Hovel, Harold J., Semiconductors and Semimetals: Solar Cells, Academic Press, New York, 1975.

Picciano, W. T., "Determination of the Solar Cell Equation, from Empirical Data," Energy Conversion, Vol. 9, Pergamon Press, Great Britain, 1969.

Rappaport, Paul, "The Photovoltaic Effect," RCA Review, Vol. 20, September 1959.

Streetman, B. G., Solid State Electronic Devices, Englewood Cliffs, New Jersey, Prentice Hall, Inc., 1972.

Sze, S. M., Physics of Semiconductors, John Wiley and Sons, Interscience, New York, 1969.

Wysocki, Joseph J., and Paul Rappaport, RCA Laboratories, "Effect of Temperature on Photovoltaic Solar Energy Conversion," Journal Applied Physics, Vol. 31, March 1960.